J. Fluid Mech. (2005), *vol.* 523, *pp.* 307–337.
DOI: 10.1017/S0022112004002113 Printed in the United Kingdom

Analytical solutions for rotating vortex arrays involving multiple vortex patches

By DARREN CROWDY AND JONATHAN MARSHALL

Department of Mathematics, Imperial College of Science, Technology and Medicine, 180 Queen's Gate, London, SW7 2AZ, UK

(Received 20 January 2004 and in revised form 3 September 2004)

A continous two-parameter family of analytical solutions to the Euler equations are presented representing a class of steadily rotating vortex arrays involving $N+1$ interacting vortex patches where $N \geqslant 3$ is an integer. The solutions consist of a central vortex patch surrounded by an N-fold symmetric alternating array of satellite point vortices and vortex patches. One of the parameters governs the size of the central patch, the other governs the size of the N satellite patches. In the limit where the areas of the satellite vortex patches tend to zero, the solutions degenerate to the exact solutions of Crowdy (*J. Fluid Mech.* vol. 469, 2002, p. 209). Limiting states are found in which cusps form only on the central patch, only on the satellite patches, or simultaneously on both central and satellite patches. Contour dynamics simulations are used to check the mathematical solutions and test their robustness. The linear stability of a class of 'point-vortex models' (in which the patches are replaced by point vortices) are also studied in order to examine the stability of the distributed-vorticity configurations to pure-displacement modes. On the other hand, a desingularization of all point vortices to Rankine vortices leads to a class of 'quasi-equilibria' consisting purely of interacting vortex patches close to hydrodynamic equilibrium.

1. Introduction

The study of vortical solutions of the incompressible Euler equations is of perennial interest to fluid dynamicists. The subject now possesses an armoury of analytical techniques aimed at gaining a theoretical understanding of the mathematics of vorticity. Newton (2001) provides one of the most comprehensive and up-to-date surveys of the available analytical techniques. A more classical treatment is given by Saffman (1992).

When modelling the dynamics of vorticity, point vortex models are by far the most common and have been valuable in advancing our knowledge of vortex dynamics. The literature in this area is wide and varied. Aref *et al.* (2002) provide a detailed review which highlights some of the important new developments. The degree of mathematical simplication is high, the tracking of vorticity being reduced to calculating the evolution of a point set. Despite these simplications, such models are highly effective.

On the other hand, any other model of vorticity usually necessitates numerical treatment from the outset. While computational vortex methods are now highly sophisticated, analytical solutions still have an important role to play. In particular, exact solutions involving distributed vorticity are significant, but few are known.

Perhaps the most famous exact solution for a uniform vortex patch is the Kirchhoff ellipse (Lamb 1993), a solution which has been generalized in a number of directions by various authors (see chap. 9 of Saffman (1992) for references). Despite their rarity, even a brief survey of the literature reveals that such exact solutions have played pivotal roles in the theoretical development of the subject. Exact solutions provide tractable leading-order models, they are paradigmatic solutions to which other physical effects can be added and studied (e.g. perturbatively or numerically), they can be used to check numerical codes and validate approximate models, they can form the basis for more complex models of multi-vortex interactions (Melander, Zabusky & Styczek 1986) or even constitute component models for the fine-scale structure of turbulence (Saffman & Pullin 1996). For all these reasons, not to mention their mathematical tractability, exact solutions are important and valuable. This paper presents an addition to this small compendium of exact solutions of the Euler equation.

Motivated by the observation of 'multipolar vortices' (Carnevale & Kloosterziel 1994; Morel & Carton 1994), Crowdy (1999) has devised an analytical method of constructing models of these vortical structures. The method relies on consideration of streamfunctions of the form

$$\psi(x, y) = \begin{cases} -\dfrac{\omega}{4}\left(z\bar{z} - \displaystyle\int^{z} S(z')\mathrm{d}z' - \int^{\bar{z}} \overline{S}(z')\mathrm{d}z'\right), & z \in D, \\ 0, & z \notin D, \end{cases} \tag{1.1}$$

where D is some vortical region and $S(z)$ is the Schwarz function (Davis 1974) of the vortex jump at the boundary ∂D. The Schwarz function of an analytic curve ∂D is the function, locally analytic in an annular neighbourhood containing the curve, satisfying

$$S(z) = \bar{z} \tag{1.2}$$

everywhere on the curve. With $S(z)$ thus defined, a function of the form (1.1) is known as a *modified Schwarz potential* (Shapiro 1992). For certain special choices of the vortical region D, Crowdy (1999) has shown that streamfunctions having the form of modified Schwarz potentials can yield equilibrium solutions of the Euler equation. Moreover, the boundaries of these special choices of D can be parameterized explicitly using conformal mappings. This leads to solutions of the Euler equation describable in analytical form.

The general idea of considering streamfunctions of the form (1.1) has proved to be versatile, leading to a range of exact solutions for vortical equilibria including a class of rotating vortex arrays in which a central vortex patch is surrounded by an N-fold symmetric distribution of point vortices (Crowdy 2002). The latter solutions generalize the classical work on N-polygonal arrays of co-rotating point vortices (initiated by Thomson (1883) and generalized by Havelock (1931) and Morikawa & Swenson (1971), among others) by introducing a finite-area vortex patch at the centre of the polygonal configuration. In turn, the present paper presents a further generalization of the solutions of Crowdy (2002) by finding equilibria in which some of the satellite point vortices have been replaced by finite-area vortex patches leading to vortical equilibria involving interacting patches. In a numerical study, Dritschel (1985) has considered the case where there is no central vortex patch, but where the N satellite point vortices are replaced by patches.

The streamline pattern of the $N = 4$ solution of Crowdy (2002) is reproduced in figure 1. This solution has a central vortex patch surrounded by four identical satellite

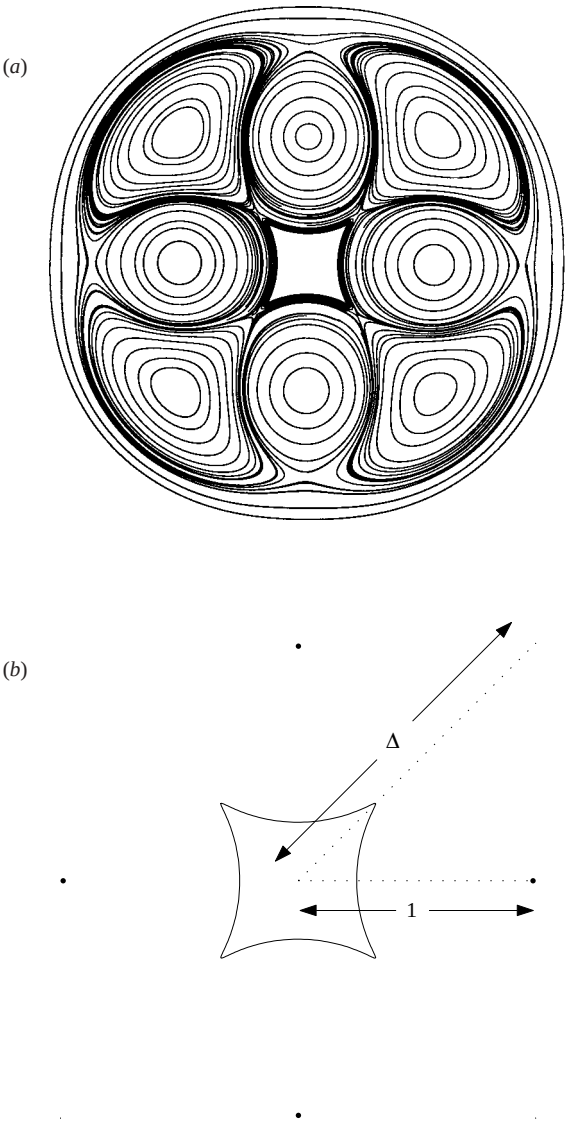

FIGURE 1. (*a*) A reproduction of figure 6 of Crowdy (2002) showing the streamline pattern associated with a central vortex patch surrounded by four satellite point vortices centred on the x- and y-axes. In the notation of Crowdy (2002), the figure corresponds to the parameter choice $a = 2.8$. Note the appearance of four 'umbrella' regions that have a 'co-rotation' point at their centre. As illustrated in (*b*), the distances of these co-rotation points and the satellite point vortices from the centroid of the central patch are Δ and 1, respectively.

point vortices. It is clear from the figure that there are eight recirculating regions with closed streamlines surrounding the central vortex patch – four associated with the four satellite point vortices and another four associated with what Dritschel (1985) has called 'umbrella regions'. There is no vorticity in these umbrella regions. They are regions of 'ghost vorticity' associated with the fact that the streamlines are being viewed in a rotating frame of reference.

It should be clear from figure 1 that at the centre of each of these umbrella regions there are points which, in the co-rotating frame, are stagnation points of the flow. Aref & Vainchtein (1998) refer to these as 'co-rotation points' since, in the laboratory frame, they co-rotate about the origin with the same angular velocity as the rest of the vortical configuration. This paper examines the possibility of constructing generalized solutions where a small patch of uniform vorticity is 'grown' at these co-rotating points. Aref & Vainchtein (1998) proposed a similar idea when they considered whether it is possible to grow new (and initially weak) point vortices at the given co-rotation points of some known point-vortex equilibrium. When this proved possible, they succeeded in finding more complex point-vortex equilibria, including asymmetric ones (Aref & Vainchtein 1998). A nonlinear continuation procedure in the circulation of these nascent point vortices was performed, with this circulation initially taken to be zero. Here, a similar continuation procedure is performed, this time in the area (initially zero) of the nascent vortex patches. This paper documents a new class of analytical solutions constructed in this way.

The new solutions have intriguing properties. Depending on the relative circulations of the central patch, the satellite patches and the satellite point vortices, we find limiting states in which the central patch exhibits cusps, but the satellite patch boundaries remain regular, limiting states where the satellite patch boundaries develop cusps, but the central patch boundary remains regular and, finally, a critical state where these two branches of solution come together leading to simultaneous cusp formation in the boundaries of both central and satellite vortex patches.

Vortex arrays, or 'vortex crystals' of the kind found here have a number of applications as surveyed by Aref *et al.* (2002). They have astrophysical and geophysical applications. Morikawa & Swenson (1971), for example, studied the case of adding a central point vortex to the N-polygonal Thomson arrays with a view to modelling storm systems around the polar vortex (modelled by the central point vortex). Later, further applications of such models to atmospheric pressure systems were considered by Bauer & Morikawa (1976). Beyond hydrodynamics, vortex arrays of the kind considered here arise as self-organized structures in non-neutral plasmas (Schecter *et al.* 1999; Durkin & Fajans 2000), a physical system which has identical governing equations.

The layout of the paper is as follows. In § 2, the ideas presented in Crowdy (1999) are generalized to the case where the configuration consists of multiple vortex patches. This reduces the problem to the construction of a special class of vortex-patch regions whose boundaries have Schwarz functions possessing special properties. These regions are most conveniently reconstructed using conformal maps and § 3 discusses such maps, revealing them to be given by automorphic functions. In § 4, the form of the required maps is given (with the mathematical details of the construction relegated to an Appendix) and shown to depend on five real parameters for any fixed $N \geqslant 3$ (the degree of symmetry). To yield an equilibrium, these five parameters must satisfy three constraints leading ultimately to a continuous two-parameter family of solutions. One of these parameters governs the size of the satellite vortex patches, the other governs the size of the central patch. The space of solutions, and the various limiting states, are discussed in detail. As a check on the mathematical construction, § 5 uses the numerical procedure of contour dynamics, with the new solutions as initial conditions, to verify that they are indeed equilibria which rotate steadily without change of form. The robustness of the structures is also examined and a class of 'point-vortex models' presented to test the stability of the structures to displacement-mode instabilities. Finally, in § 6, the possibility of finding pure-patch equilibria by desingularizing the point vortices in the new equilibria is studied.

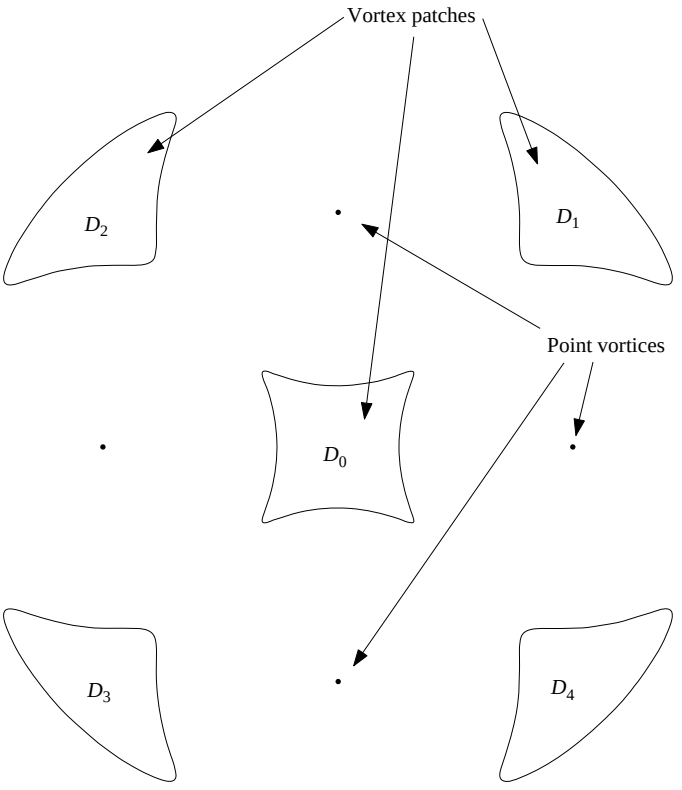

FIGURE 2. Schematic showing the vortex configurations under consideration in the case $N = 4$. A central vortex patch is surrounded by an alternating distribution of N point vortices and N satellite vortex patches. The configuration is steadily rotating. The central vortex patch is D_0, the N satellite patches are $\{D_j | j = 1, \ldots, N\}$. The region exterior to these patches is D and is in irrotational motion except for N point vortices.

2. Mathematical formulation

Consider an unbounded fluid region D exterior to a central vortex patch D_0 and N satellite vortex patches $\{D_j | j = 1, \ldots, N\}$. All vortex patches are taken to have uniform vorticity $\tilde{\omega}$. The centroids of the satellite vortices are on the rays

$$\arg[z] = \pi(1 + 2j)/N \quad (j = 0, 1, \ldots, N - 1), \tag{2.1}$$

so that the configuration has an N-fold rotational symmetry about the centroid of the central patch. Suppose also that, alternating between the vortex patches, there is a distribution of N point vortices. For an N-fold symmetric vorticity distribution, these point vortices must lie on the rays

$$\arg[z] = 2\pi j/N \quad (j = 0, 1, \ldots, N - 1). \tag{2.2}$$

Let the point-vortex positions be $\{z_j | j = 1, \ldots, N\}$. Apart from these singularities, the fluid in D is assumed to be in irrotational motion. Figure 2 shows a diagram of the special case $N = 4$ which will be treated in detail in what follows.

We seek solutions in which all vortex patches and point vortices have the same angular velocity $\tilde{\omega}/2$ about the centroid of the central patch. Furthermore, the fluid inside all vortex patches will be taken to be in pure solid-body rotation. This means

that, in a frame of reference co-rotating with the configuration, the fluid inside all the vortex patches is stagnant. While such solutions are clearly a subclass of all possible solutions, it will be seen that they are the ones which can be described in analytical form.

Motivated by the analysis in Crowdy (2002), we now pose that the streamfunction of such a flow, in a frame of reference co-rotating with the configuration, is of the form

$$\psi(x,y) = \begin{cases} \dfrac{\tilde{\omega}}{4}\left(z\bar{z} - \displaystyle\int^{z} S(z')\mathrm{d}z' - \int^{\bar{z}} \overline{S}(z')\mathrm{d}z' \right), & z \in D, \\ 0, & z \notin D, \end{cases} \tag{2.3}$$

where $S(z)$ is the Schwarz function (if it exists) of all the boundaries of D, i.e. $\{\partial D_j | j = 0, 1, \ldots, N\}$. This means that it must be locally analytic in annular neighbourhoods of all boundaries $\{\partial D_j | j = 0, 1, \ldots, N\}$ and must satisfy the $N+1$ conditions

$$S(z) = \bar{z} \quad \text{on} \quad \partial D_j \quad (j = 0, 1, \ldots, N). \tag{2.4}$$

It is easily verified that (2.3) satisfies

$$\nabla^2 \psi = 4\psi_{z\bar{z}} = \tilde{\omega} \tag{2.5}$$

everywhere in D, except possibly at any singularities of $S(z)$. This uniform vorticity in D is associated with ψ in (2.3) being the streamfunction in a frame of reference co-rotating with angular velocity $\tilde{\omega}/2$.

If there are N point vortices in D, an additional condition on $S(z)$ is that it must be analytic in D except for simple poles. The velocity field associated with (2.3) is

$$u - \mathrm{i}v \equiv 2\mathrm{i}\psi_z = \frac{1}{2}\mathrm{i}\tilde{\omega}(\bar{z} - S(z)), \tag{2.6}$$

so simple poles of $S(z)$ do indeed correspond to point vortices.

A kinematic condition to be satisfied is that all vortex patch boundaries are streamlines. A dynamic condition is that the fluid pressure is continuous at all vortex jumps. It is well known (Saffman 1992) that this dynamic condition is equivalent to the continuity of the velocity across the vortex-patch boundaries.

To examine whether these two boundary conditions can be satisfied, observe that, if $S(z)$ satisfies (2.4) on $\{\partial D_j | j = 0, 1, \ldots, N\}$, it is easy to see that the streamfunction (2.3) satisfies the dynamic condition because $u - \mathrm{i}v$, as given in (2.6), vanishes on all the patch boundaries and is therefore continuous with the stagnant flow inside the patches. The kinematic condition is also satisfied by (2.3) since, on use of (2.4) and (2.6),

$$\mathrm{d}\psi = \psi_z \mathrm{d}z + \psi_{\bar{z}}\mathrm{d}\bar{z} = 0 \quad \text{on} \quad \partial D_j \quad (j = 0, 1, \ldots, N). \tag{2.7}$$

Thus, provided a domain D and a corresponding function $S(z)$ satisfying the above conditions can be found, the streamfunction (2.3) satisfies both the kinematic and dynamic conditions on the vortex-patch boundaries. It then only remains to ensure that all the point vortices (corresponding to the N simple poles of $S(z)$) are stationary under the effects of the non-self-induced velocity field. This is a requirement, dictated by the Helmholtz laws of vortex motion (Saffman 1992), for a consistent steady solution of the Euler equation.

3. Conformal mapping

Two things remain to be determined. (i) Does there exist a function $S(z)$ and domain D satisfying the requirement (2.4) and the condition that $S(z)$ has just N simple poles in D? (ii) If so, can all the point vortices be made steady under the effects of their non-self-induced velocities? This section deals with the first of these questions by showing how to parameterize, using conformal maps, the boundaries of the special class of domains D for which $S(z)$ has all the properties required above.

It is convenient to introduce a conformal mapping $z(\zeta)$ from some pre-image domain H in a parametric ζ-plane to the unbounded region D. In contrast to the case of a single vortex patch considered in Crowdy (2002), because there are now multiple vortex patches involved, the region D is multiply connected. The pre-image region H must therefore also be multiply connected. The Riemann mapping theorem guarantees the existence of a conformal map from some pre-image region H. This time, however, H is not completely determined *a priori*, but depends on certain adjustable parameters which must be determined as part of the construction.

Suppose that a region H in a parametric ζ-plane maps to D. Here, we take H to be the unit ζ-disk with N smaller circular disks excised. Let these smaller circular disks be $\{H_j | j = 1, \ldots, N\}$ and let their respective circular boundaries be $\{\partial H_j | j = 1, \ldots, N\}$. Also, let the unit circle $|\zeta| = 1$ be denoted ∂H_0. In a natural way, the pre-image circles $\{\partial H_j | j = 1, \ldots, N\}$ will map to the boundaries $\{\partial D_j | j = 1, \ldots, N\}$ of the N satellite patches, while ∂H_0 will map to the boundary ∂D_0 of the central patch. Let $\{\delta_j | j = 1, \ldots, N\}$ denote the centres of these circular disks and let $\{q_j | j = 1, \ldots, N\}$ denote their radii.

The region H is bounded, but it maps to an unbounded region D. $z(\zeta)$ must therefore have a single simple pole in H (the pole must be simple because the mapping function must be one-to-one; a higher-order pole would yield a multi-valued mapping function). By the symmetry of the configuration, it is natural to let $\zeta = 0$ map to physical infinity. Apart from this simple pole, $z(\zeta)$ must be analytic everywhere else in H and, moreover, z_ζ must vanish nowhere in H. This is a necessary (but not sufficient) condition for $z(\zeta)$ to be a one-to-one map. If $z(\zeta)$ is one-to-one then it can, in principle, be inverted to find ζ as a single-valued function of z, i.e. $\zeta = \zeta(z)$.

Given the N-fold rotational symmetry of the fluid region D, it is reasonable to seek a pre-image region H which shares these symmetries. We therefore take

$$\delta_j = \delta \exp((1 + 2(j-1))\mathrm{i}\pi/N), \quad q_j = q \quad \text{for } j = 1, \ldots, N. \tag{3.1}$$

That is, the centres of the circular disks $\{H_j | j = 1, \ldots, N\}$ are assumed to be disposed in an N-fold symmetric fashion about $\zeta = 0$ at distance δ from the origin and all are taken to have radius q. Figure 3 shows a schematic of the pre-image region in the case $N = 4$ relevant to the vortex configuration in figure 2. Whatever the value of N, the shape of the associated pre-image domain H is completely known except for only the two unknown real parameters δ and q. These two parameters are to be determined as part of the solution.

On ∂H_0,

$$\bar{z} = \overline{z(\zeta)} = \bar{z}(\bar{\zeta}) = \bar{z}(\zeta^{-1}) \tag{3.2}$$

where we have made use of the fact that $\bar{\zeta} = \zeta^{-1}$ on ∂H_0. Given that $\zeta = \zeta(z)$, $\bar{z}(\zeta^{-1})$ effectively defines some new function of z which we shall call $S_0(z)$. Notice from (3.2) that $S_0(z)$ equals $\bar{z}$ everywhere on ∂D_0.

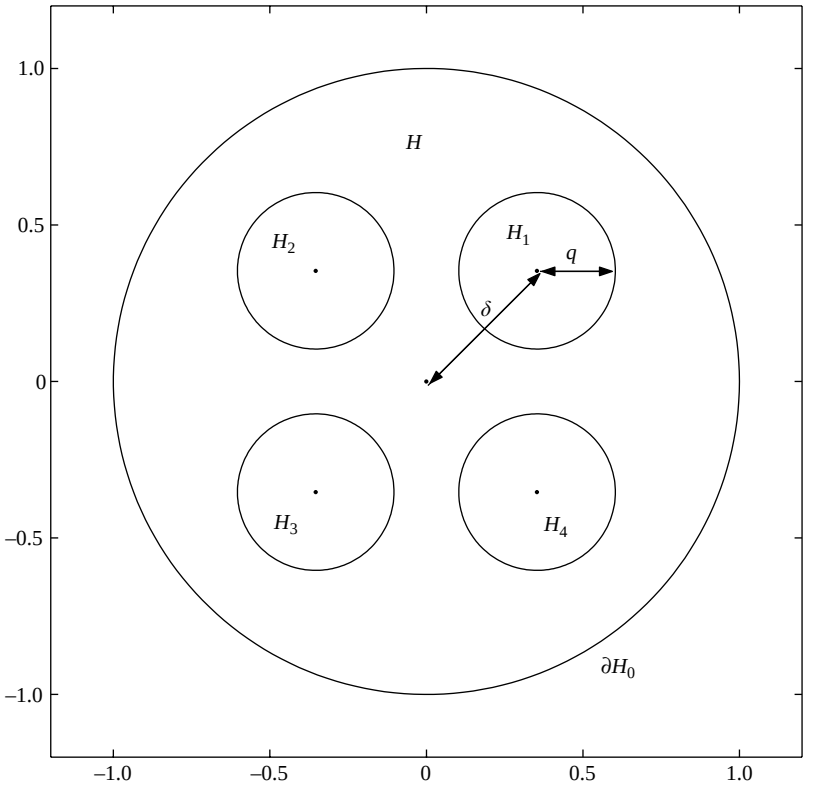

FIGURE 3. Schematic of pre-image ζ-plane for $N = 4$ showing region H consisting of unit ζ-disk with four equal excised disks, of radius q, with centres at $\delta e^{(\pi i(2j-1)/4)}$, $j = 1, 2, 3, 4$. The point $\zeta = 0$ maps to $z = \infty$. When $q = 0$, the disks H_j disappear, the pre-image domain is just the unit ζ-circle and the mappings (4.1) reduce to the rational function conformal maps of Crowdy (2002) describing configurations with no satellite patches.

Next, on ∂H_j,

$$|\zeta - \delta_j|^2 = (\zeta - \delta_j)(\bar{\zeta} - \bar{\delta}_j) = q_j^2, \tag{3.3}$$

or, on rearrangement,

$$\bar{\zeta} = \bar{\delta}_j + \frac{q_j^2}{\zeta - \delta_j} \equiv \phi_j(\zeta) \quad \text{for } j = 1, \ldots, N, \tag{3.4}$$

an expression which defines N conformal maps $\phi_j(\zeta)$. Each of these maps can be written in the form

$$\phi_j(\zeta) = \frac{a_j\zeta + b_j}{c_j\zeta + d_j} \tag{3.5}$$

for some complex constants a_j, b_j, c_j and d_j. Maps of the general form (3.5) are known as Möbius maps (Ablowitz & Fokas 1997). On ∂H_j, we therefore have

$$\bar{z} = \overline{z(\zeta)} = \bar{z}(\bar{\zeta}) = \bar{z}(\phi_j(\zeta)), \tag{3.6}$$

where we have used (3.4) in the last step. Again, given that $\zeta = \zeta(z)$, $\bar{z}(\phi_j(\zeta))$ each defines some function of z which will be called $S_j(z)$. An inspection of (3.6) reveals that $S_j(z) = \bar{z}$ on the boundary ∂D_j.

However, the final function $S(z)$ which we seek must be equal to $\bar{z}$ on all the $N+1$ boundaries $\{\partial D_j | j = 0, 1, \ldots, N\}$. This will certainly be satisfied if we can find a single function $S(z)$ such that

$$S(z) = S_0(z) = S_j(z) \quad \text{for } j = 1, \ldots, N. \tag{3.7}$$

By (3.2) and (3.6), this implies that the mapping $z(\zeta)$ must satisfy

$$\bar{z}(\zeta^{-1}) = \bar{z}(\phi_j(\zeta)) \quad \text{for } j = 1, \ldots, N. \tag{3.8}$$

Equivalently, letting $\zeta \mapsto \zeta^{-1}$ in (3.8) and taking complex conjugates,

$$z(\zeta) = z(\theta_j(\zeta)) \quad \text{for } j = 1, \ldots, N \tag{3.9}$$

where the new maps θ_j, $j = 1, \ldots, N$ are defined as

$$\theta_j(\zeta) \equiv \overline{\phi}_j(\zeta^{-1}) = \delta_j + \frac{q_j^2 \zeta}{(1 - \bar{\delta}_j \zeta)}. \tag{3.10}$$

The maps $\{\theta_j(\zeta) | j = 1, \ldots, N\}$ are also Möbius maps.

The condition that $S(z)$ has only simple pole singularities at the points $\{z_j | j = 1, \ldots, N\}$ inside D implies that $\bar{z}(\zeta^{-1}) = S_0(z) = S(z)$ has simple pole singularities at the points ζ_j where ζ_j denotes the point inside H mapping to z_j, i.e.

$$z(\zeta_j) = z_j, \quad \text{for } j = 1, \ldots, N. \tag{3.11}$$

It follows that $z(\zeta)$ must have N simple pole singularities at the points $\{\bar{\zeta}_j^{-1} | j = 1, \ldots, N\}$. These are outside the region H.

A function which is invariant when its argument undergoes a transformation given by a finite set of Möbius maps (i.e. functions satisfying a set of conditions of the form (3.9)) is known as an *automorphic function* (Baker 1995; Ablowitz & Fokas 1997). By the above, the required conformal mapping functions are therefore given by automorphic functions. In the next section, we explicitly present the relevant class of conformal mappings producing the required N-fold symmetric distribution of vortex patches as the image domains. These mappings have been constructed using the general theory of automorphic functions (see Baker (1995) or Crowdy & Marshall (2004*a*)).

4. Exact solutions

The form of the required conformal mapping functions can be stated in terms of a single special function of ζ which is defined in Appendix A and denoted $\omega(\zeta, \gamma)$ where γ is some complex parameter. Explicitly, the required conformal maps are

$$z(\zeta) = R \frac{\omega(\zeta, \infty)\omega_N(\zeta, \beta)}{\omega(\zeta, 0)\omega_N(\zeta, \alpha)}, \tag{4.1}$$

where α, β and R are real parameters and where $\omega_N(\zeta, \gamma)$ is a product of N of these new special functions given by

$$\omega_N(\zeta, \gamma) = \prod_{j=1}^{N} \omega(\zeta, \gamma \exp(2\pi \mathrm{i}(j-1)/N)). \tag{4.2}$$

An important fact about $\omega(\zeta, \gamma)$ is that it has a simple zero at $\zeta = \gamma$. Note from its denominator that, as required, the function (4.1) has a simple pole at $\zeta = 0$ (the point mapping to physical infinity) and at the N points $\{\alpha e^{2\pi \mathrm{i}(j-1)/N} | j = 1, \ldots, N\}$ which

correspond to the N simple poles of the map discussed at the end of the previous section. In order that these poles are outside H, we take $\alpha > 1$.

As might be expected, the definition of $\omega(\zeta, \gamma)$ requires knowledge of the N Möbius maps $\{\theta_j | j = 1, \ldots, N\}$. It is defined as an infinite product. Its definition and explicit construction in the special case $N = 4$ is given in Appendix A. The construction for all other N is analogous. For any N, these N Möbius maps depend only on the two parameters q and δ characterizing the pre-image domain H.

While vortical solutions have been found to exist for all integers $N \geqslant 3$ (note that the solutions of Crowdy (2002) were only found to exist for $N \geqslant 3$), for clarity, we have elected to present only the solutions for $N = 4$ in detail. The four Möbius maps $\{\theta_1, \theta_2, \theta_3, \theta_4\}$ required to define $\omega(\zeta, \gamma)$ in this case depend on the two real parameters q and δ (Appendix A gives these four maps explicitly). The map (4.1) therefore depends on a total of five real parameters

$$q, \delta, R, \alpha, \beta. \tag{4.3}$$

These must satisfy a single constraint which we call the *automorphicity condition* because it is the condition required to ensure that (4.1) satisfies (3.9). R is simply a normalization parameter and can be chosen as required. Here, we specify that the satellite point vortices are unit distance from the centroid of the central vortex patch. This will be referred to as the *normalization condition.*

Given these two conditions, there remain three undetermined real parameters in the conformal map. It turns out that two of these can be chosen freely. Once chosen, the final parameter must be determined by the requirement that the four satellite point vortices are stationary under the effects of the local non-self-induced velocity field. Owing to the symmetry of the configuration, there is only a single such condition because ensuring that any one of the satellite point vortices is stationary automatically ensures that they are all stationary. We shall call this the *stationarity condition.* Appendix B gives a formula for this stationarity condition as a function of the conformal mapping parameters.

The two parameters that we shall pick freely will be α and q. Once chosen, R, δ and β are then determined by the automorphicity condition, the normalization condition and the stationarity condition. If, for a given α and q, these three conditions can be simultaneously satisfied and the resulting conformal map is a one-to-one map from H to some region D, then an exact solution of the Euler equation is the result.

Using the fact that $S(z) = \bar{z}(\zeta^{-1})$, it is clear that $S(z)$ has poles at $\zeta = \pm\alpha^{-1}, \pm\mathrm{i}\alpha^{-1}$ which are all inside H. The four point vortices are therefore at $z(\pm\alpha^{-1})$ and $z(\pm\mathrm{i}\alpha^{-1})$ in the physical plane. It is useful to think of the parameter α as governing the size of the central vortex patch while q governs the size of the satellite patches. Indeed, when $q = 0$, the circles $H_1, \ldots, H_4$ in the ζ pre-image plane degenerate to the points δ_j, $j = 1, \ldots, 4$ and the satellite vortex patches in the physical plane similarly degenerate to points. As discussed in § 1, we expect these points in the physical plane to be precisely the co-rotation points at the centres of the umbrella regions shown in figure 1.

There is an analytical connection with the $N = 4$ solutions of Crowdy (2002) that proves useful in the construction of the generalized solutions. It is easy to show that, when $q = 0$, the special function $\omega(\zeta, \gamma)$ degenerates to

$$\omega(\zeta, \gamma) = (\zeta - \gamma), \tag{4.4}$$

so that, in turn, (4.1) degenerates to a simple rational function. With the circular disks $H_1, \ldots, H_4$ having disappeared (because their radius q is zero) the pre-image

region H reduces to the interior of the unit ζ-circle. Then, the resulting rational function is precisely the rational function conformal map identified by Crowdy (2002) giving solutions for a central vortex patch with four co-rotating point vortices (and no satellite patches). In that case, the conformal map from the interior of the unit ζ-circle is

$$z(\zeta) = \tilde{R}\left(\frac{1}{\zeta} + \frac{b\zeta^3}{\zeta^4 - a^4}\right), \tag{4.5}$$

where $\tilde{R}, a$ and b are real parameters. The correspondence of these parameters with those of the present study is given by

$$\begin{aligned} \alpha &= a, \\ \beta &= \frac{a}{(1+b)^{1/4}}, \\ R &= \tilde{R}(1+b). \end{aligned} \tag{4.6}$$

This correspondence is useful in constructing generalized solutions for non-zero q using a continuation procedure. We expect the centre of the circle H_1 to be at $\delta e^{i\pi/4}$ – the pre-image point of the co-rotation point $\Delta e^{i\pi/4}$ in the physical plane shown in figure 1. At this point in the co-rotating frame, $u - iv = 0$. Thus,

$$u - iv|_{\zeta=\delta e^{i\pi/4}} = \bar{z}(\bar{\zeta}) - \bar{z}(\zeta^{-1})|_{\zeta=\delta e^{i\pi/4}} = 0. \tag{4.7}$$

On use of (4.5), (4.7) yields the (real) relation

$$\frac{1}{\delta} + \frac{b\delta^3}{\delta^4 + a^4} = \delta + \frac{b\delta}{1 + a^4\delta^4}, \tag{4.8}$$

which is an equation for δ given the values of a and b. However, for given a (and N), b is given by an explicit formula derived by Crowdy (2002). The value of δ then follows by solving the single nonlinear equation (4.8). On use of the relations (4.6), we then have initial values for R, α, β and δ (corresponding to $q = 0$). Solutions for non-zero $q > 0$ are then obtained by a continuation procedure using Newton's method with the (α, β, R, δ) values relevant for $q = 0$ used as initial conditions. This procedure proves highly effective.

It is worth remarking that (4.7) and (4.8) can be viewed as generalizations of what Aref & Vainchtein (1998) refer to as *Morton's equation* (Morton 1933) for finding the co-rotation points of a point-vortex configuration. Here, (4.7) is the equation that must be solved to find the co-rotating points of a more general vortical configuration.

Figure 4 shows the (α, q)-parameter space for which equilibria have been found to exist. This choice of parameters is convenient since, roughly speaking, α governs the size (and hence circulation) of the central patch while q governs the size (and hence circulation) of the satellite patches. To see this, recall that, when $q = 0$, the solutions reduce to those of Crowdy (2002) and the parameter α corresponds to the parameter a in the latter reference (see also (4.6)). It is known that in the limit $a \to \infty$, the central patch becomes vanishingly small. As a decreases, the size of the central patch generally grows until a reaches a minimum possible value at which point the central patch has developed cusp singularities in its boundary. This minimum value is denoted $\alpha^{(4)}_{crit} = 2.565$ where this numerical value is taken from Crowdy (2002). Thus, there is a minimum possible value of a for which the central patch is so large that the limiting cuspidal state is reached. On the other hand, when $q = 0$, the satellite patches have zero area and this area is generally found to increase with increasing q. In general, it is found that equilibria exist for q values below some critical value

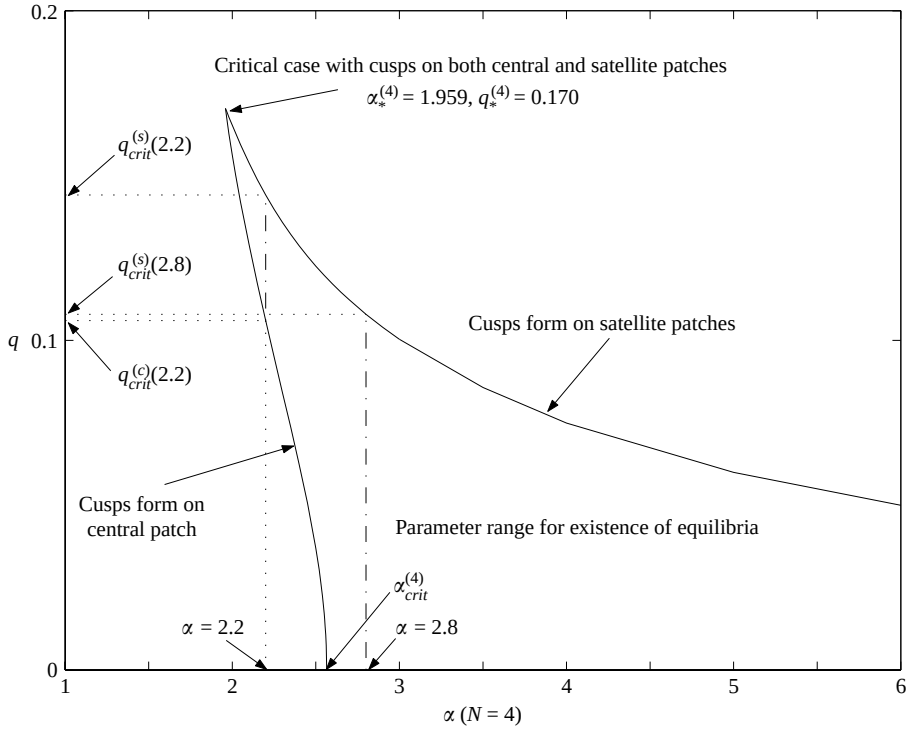

FIGURE 4. (α, q)-parameter space indicating the region where equilibria exist in the case $N = 4$. The vertical dot-dash line at $\alpha = 2.8$ shows that solutions exist for $q \in [0, q_{crit}^{(s)}(2.8)]$. Typical configurations along this dot-dash line are shown in figure 5. The vertical dot-dash line at $\alpha = 2.2$ shows that solutions exist for $q \in [q_{crit}^{(c)}(2.2), q_{crit}^{(s)}(2.2)]$. Typical configurations along this dotted line are shown in figure 7. Also clearly marked is the intersection point of the two branches of limiting solution where the limiting state exhibits cusps in the boundaries of both the central and satellite patches. This critical configuration is shown in figure 9.

where the limiting vortex configuration exhibits 3/2-cusp singularities on the satellite patches. Physically, if q is a measure of the size of the satellite patch, for fixed α, there is a limiting size to which the satellite patches can grow before they form cusp singularities in the vortex patch boundaries. This critical value of q, which is a function of α, is denoted $q_{crit}^{(s)}(\alpha)$.

If $\alpha > \alpha_{crit}^{(4)}$, it is found that equilibria exist for q-values in the interval

$$q \in \left[0, q_{crit}^{(s)}(\alpha)\right]. \tag{4.9}$$

Figure 5 shows the vortex configurations for the fixed value $\alpha = 2.8$ – which is greater than $\alpha_{crit}^{(4)} = 2.565$ – for six different choices of q in the interval

$$q \in \left[0, q_{crit}^{(s)}(2.8)\right]. \tag{4.10}$$

The circulation Γ_{cp} of the central vortex patch, the circulation Γ_{sp} of each of the satellite vortex patches and the circulation Γ_s of each of the satellite point vortices are indicated on each diagram. Appendix B gives a formula for Γ_s in terms of the conformal mapping parameters. Figure 6 shows graphs of these three circulations as continuous functions of q. Notice that Γ_{sp} (which is proportional to the area of the

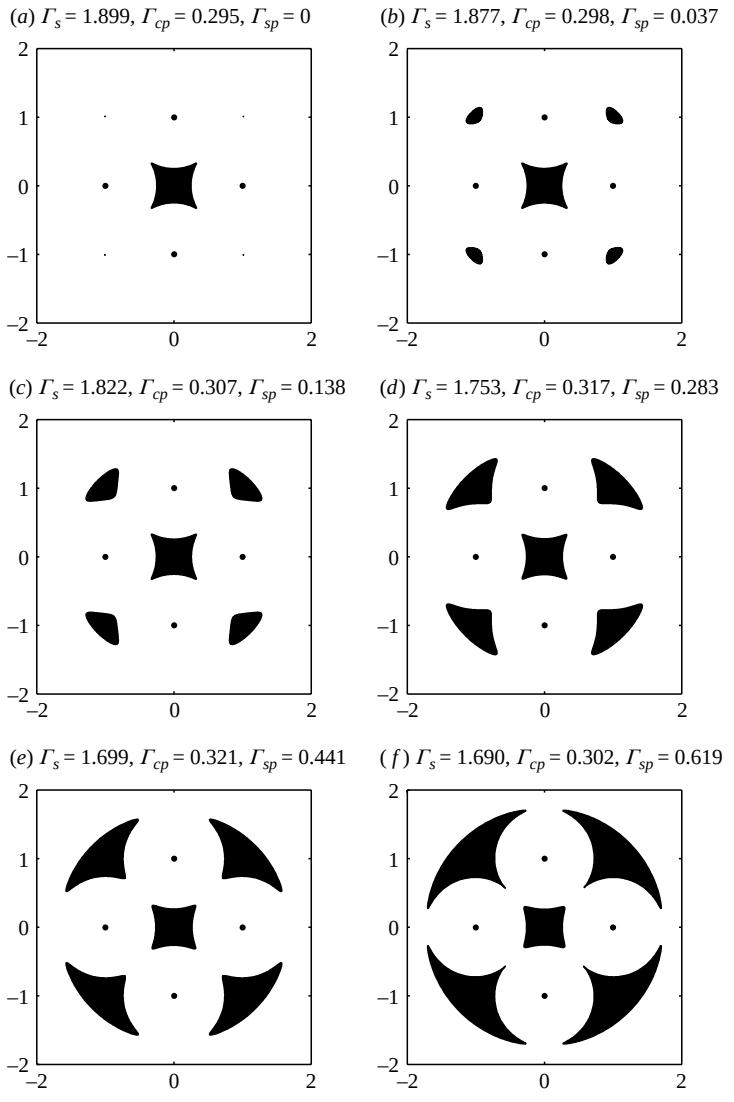

FIGURE 5. Vortical equilibria for $\alpha = 2.8$ and $q = 0, 0.02, 0.04, 0.06, 0.08$ and $q = q_{crit}^{(s)} = 0.108$. The circulations of the point vortices Γ_s, the central patch Γ_{cp} and satellite patches Γ_{sp} are shown. (*a*) shows a solution found in Crowdy (2002) (and reproduced in figure 1) and indicates (as small dots) the positions of the four 'co-rotating points' from which satellite patches can be 'grown'. (*f*) is the limiting state where four cusps form simultaneously on the satellite patches at the points closest to the central patch.

satellite patches) is a monotonically increasing function of q, thus corroborating the previous statement that q can be viewed as a parameter governing the size of the satellite vortex patches.

The choice $\alpha = 2.8$ is made because the $q = 0$ solution, shown in figure 5(*a*), coincides with the solution reproduced in figure 1. The position of the co-rotation points (or, equivalently, the centroids of the 'umbrella regions' of figure 1) are also clearly marked in this diagram. It is from these co-rotation points that it is possible to 'grow' satellite vortex patches of non-zero area, as indicated in the progression

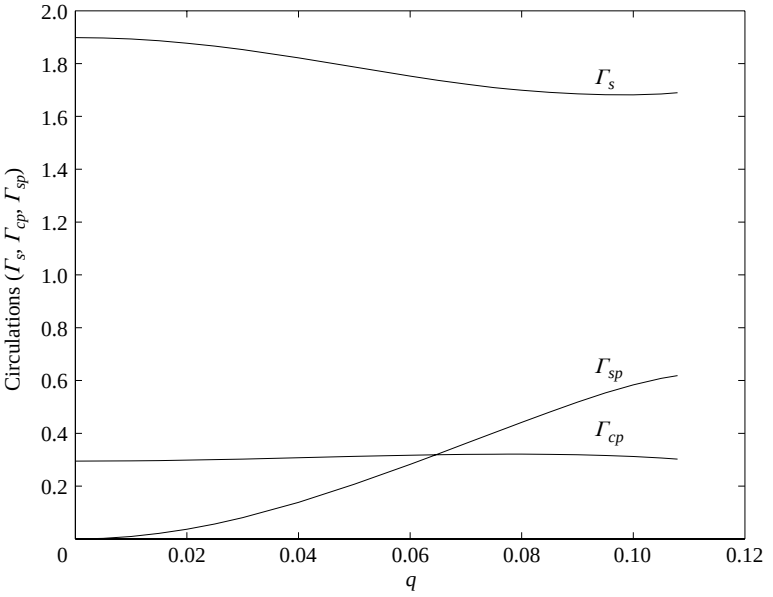

FIGURE 6. Graphs of the circulations of the point vortices Γ_s, the central patches Γ_{cp} and the satellite patches Γ_{sp} against q (abscissa) for fixed $\alpha = 2.8$. Note that Γ_{sp} starts at zero since, when $q = 0$, the patches degenerate to co-rotation points (with zero circulation).

of figure 5(*a*) to figure 5(*f*), each corresponding to successively bigger values of q. Since the boundaries of the satellite patches are streamlines, it is reassuring that they assume the same umbrella-type shape as the streamlines in the 'umbrella regions' of ghost vorticity in the rotating solutions of figure 1.

It is also found that equilibria exist for α less than $\alpha^{(4)}_{crit}$. Indeed, they exist in a range which is denoted

$$\alpha \in \left[\alpha^{(4)}_{*}, \alpha^{(4)}_{crit}\right]. \tag{4.11}$$

For α in this range it is found that, while no solutions exist for q just above zero, there is nevertheless a window of q-values for which solutions do exist. The limiting solutions are found to exhibit cusp singularities in the boundaries of either the central or the satellite vortex patches. For a fixed α in the range (4.11), this window of admissible q values (which depend on α) will be denoted

$$q \in \left[q^{(c)}_{crit}(\alpha), q^{(s)}_{crit}(\alpha)\right]. \tag{4.12}$$

The notation makes use of superscript 'c' and 's' indicating 'central' and 'satellite'; this is because it is found that the lowest admissible value of q yields a limiting state where the central patch exhibits four cusp singularities in its boundary while for the highest admissible value of q, the four satellite vortices exhibit boundary cusps. Figure 7 shows a range of vortex configurations for fixed $\alpha = 2.2$ – which is in the range (4.11) – and for six different choices of q in the interval

$$q \in \left[q^{(c)}_{crit}(2.2), q^{(s)}_{crit}(2.2)\right]. \tag{4.13}$$

This range of q values is clearly indicated by a dotted vertical line (the line $\alpha = 2.2$)

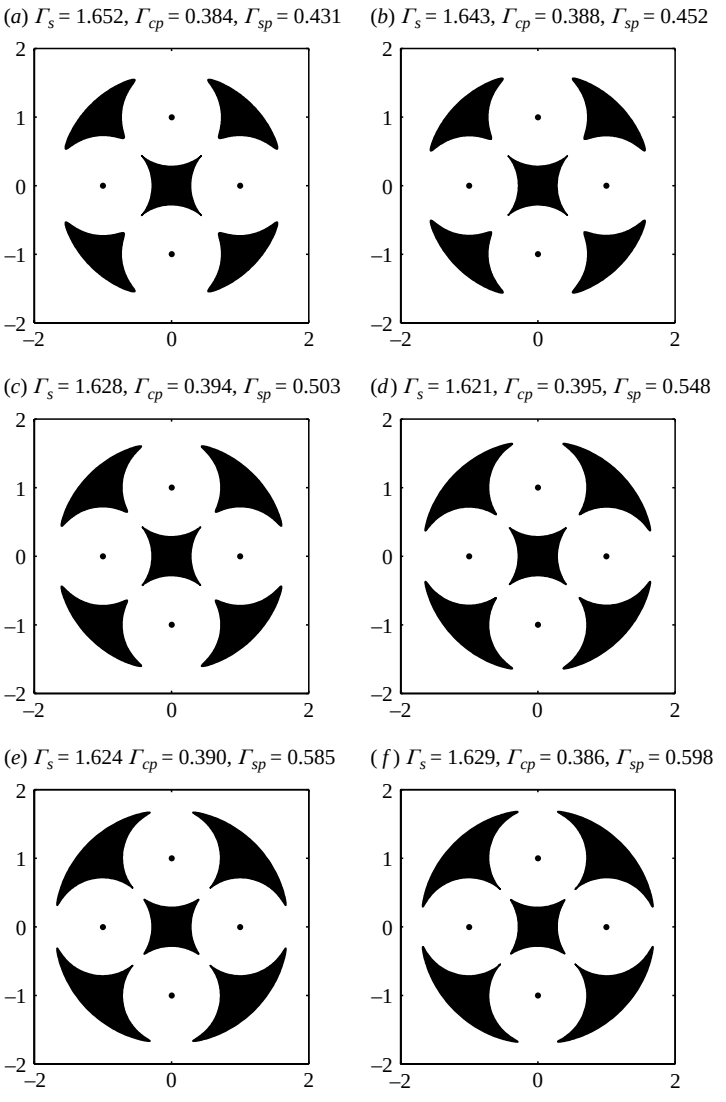

FIGURE 7. Vortical equilibria for $\alpha = 2.2$ and $q = q^{(c)}_{crit} = 0.106, 0.11, 0.12, 0.13, 0.14$ and $q^{(s)}_{crit} = 0.144$. The circulations of the point vortices Γ_s, the central patch Γ_{cp} and satellite patches Γ_{sp} are shown. In (*a*), the limiting configuration exhibits four symmetric cusps in the boundaries of the central patch while in (*f*), the limiting configuration exhibits cusps in each of the four satellite patches at the points closest to the central patch.

in figure 4 intersecting the region of parameter space where solutions exist. Graphs of the corresponding circulations Γ_{cp}, Γ_{sp} and Γ_s are shown in figure 8. Notice that Γ_{sp} is again a monotonically increasing function of q.

There exists a critical choice of parameters $\alpha = \alpha^{(4)}_*$ and $q = q^{(4)}_*$ at which the two solution branches just described meet. In the corresponding critical state, cusps form simultaneously on both the central and satellite vortex patches. This point in the (α, q)-parameter space is clearly marked in figure 4. The critical configuration is shown in figure 9. The cusps which form on the central and satellite patches in this limit do not touch each other.

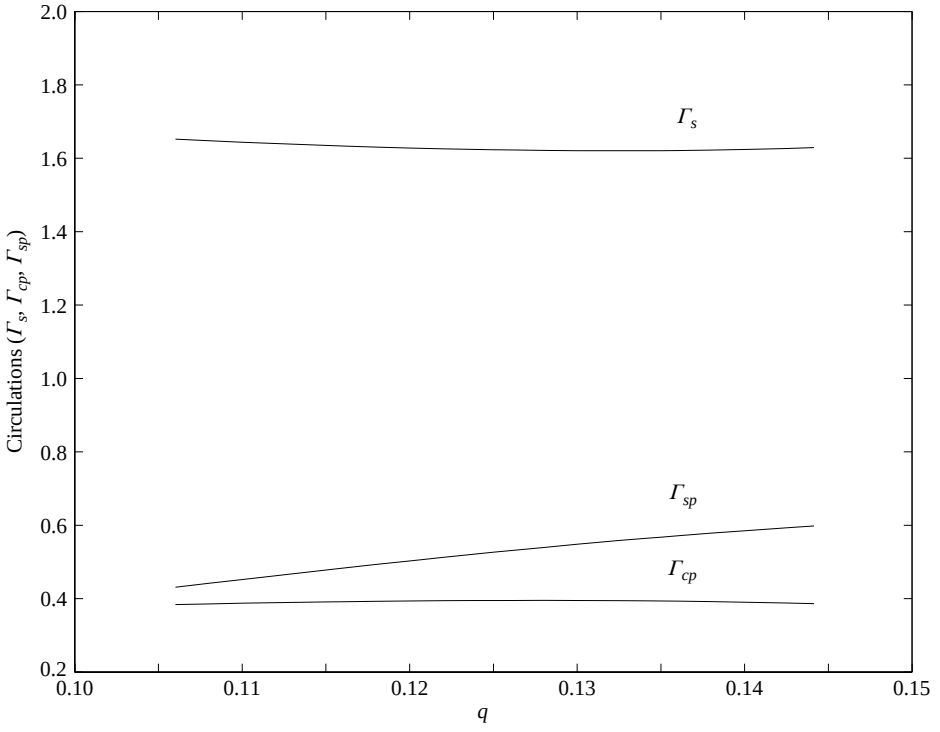

FIGURE 8. Graphs of the circulations of the point vortices Γ_s, the central patch Γ_{cp} and the satellite patch Γ_{sp} against q (abscissa) for fixed $\alpha = 2.2$.

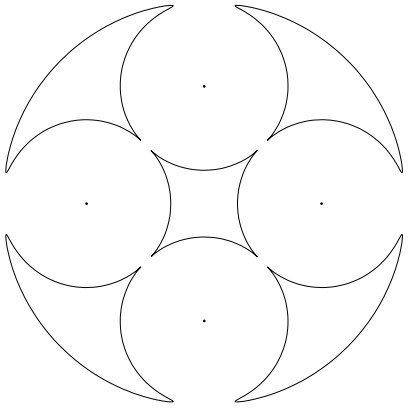

FIGURE 9. Critical configuration, exhibiting the simultaneous formation of cusps on both the central and satellite patches, corresponding to parameters $N = 4$, $\alpha = \alpha_*^{(4)} = 1.959$, $q = q_*^{(4)} = 0.170$. The cusps do not touch.

The solutions for $N = 4$ have been described in detail, but the solution structure for other N is qualitatively similar. Figure 10 shows the region of the (α, q)-parameter space for which equilibria exist in the case $N = 3$ while figure 11 shows graphs of the circulations Γ_{cp}, Γ_{sp} and Γ_s for two typical choices of α, one above $\alpha_{crit}^{(3)}$ and another below it. Figures 12 and 13 show the analogous graphs for $N = 5$. It is clear that, apart from differences in the relative sizes of the circulations in each case, the graphs for $N = 3, 4$ and 5 are qualitatively similar.

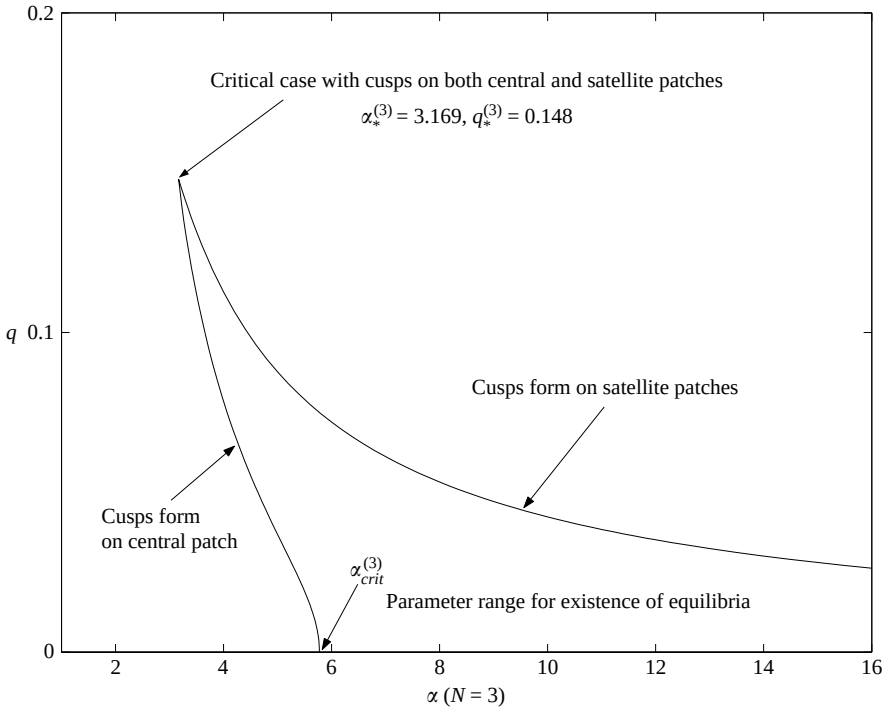

FIGURE 10. (α, q)-parameter space indicating the region where equilibria exist in the case $N = 3$.

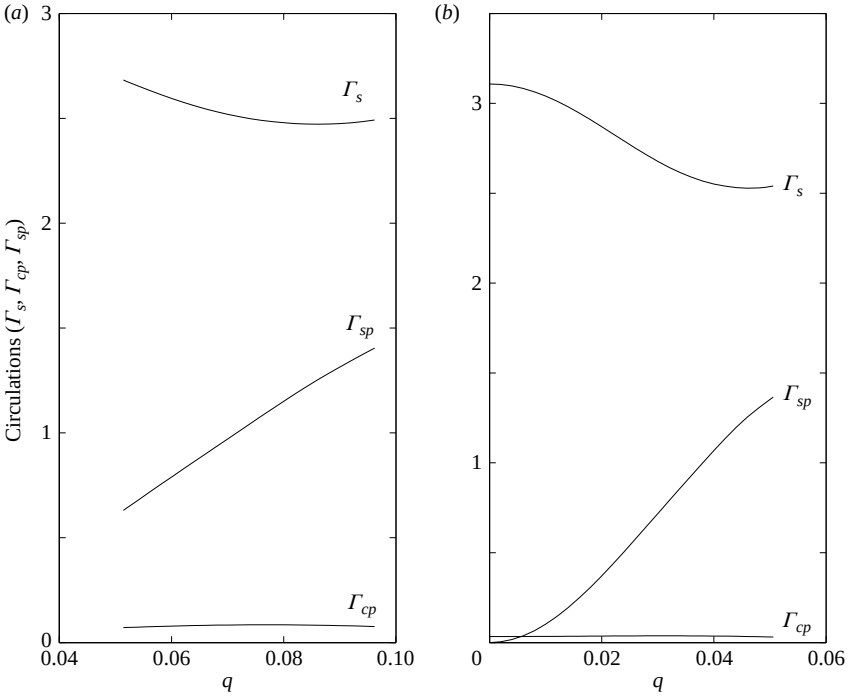

FIGURE 11. Graphs of circulations Γ_s, Γ_{cp}, Γ_{sp} against q for two different values of α on either side of $\alpha_{crit}^{(3)}$, (*a*) $\alpha = 4.6$, (*b*) 8.4.

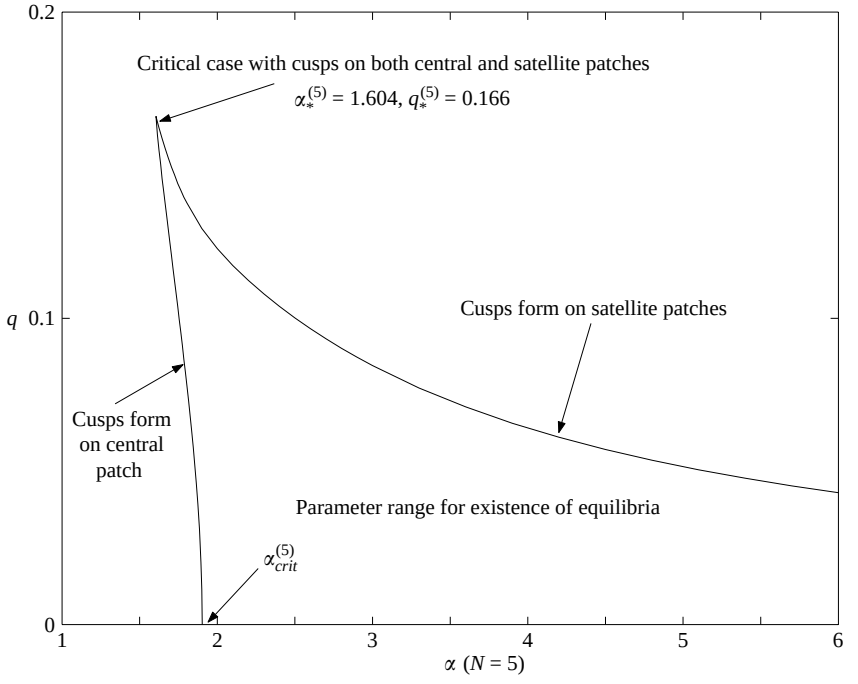

FIGURE 12. (α, q)-parameter space indicating the region where equilibria exist in the case $N = 5$.

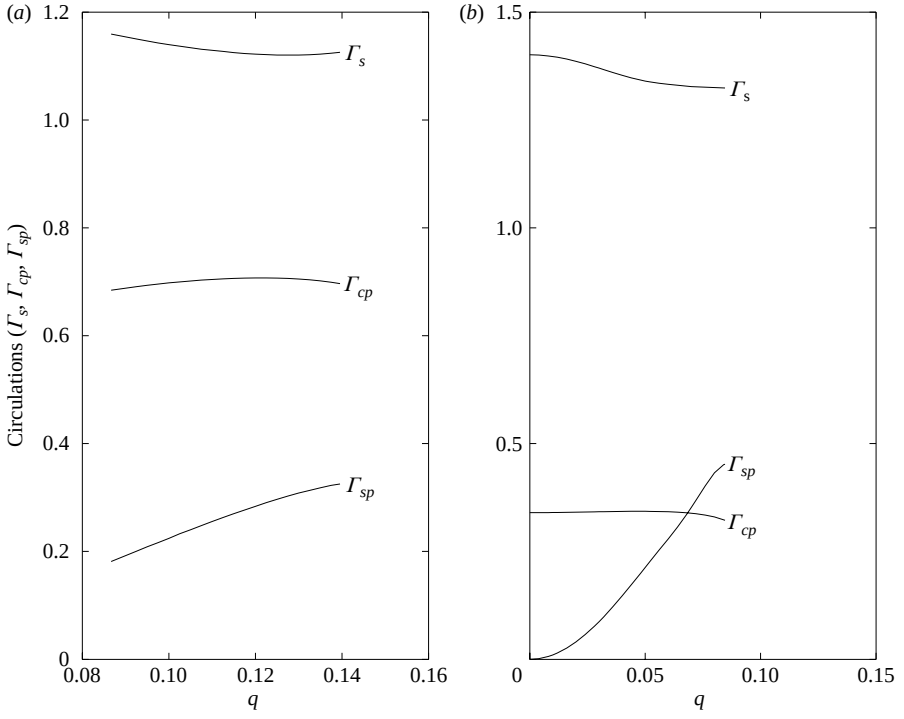

FIGURE 13. Graphs of circulations Γ_s, Γ_{cp}, Γ_{sp} against q for two different values of α on either side of $\alpha_{crit}^{(5)}$, (*a*) $\alpha = 1.785$, (*b*) 3.

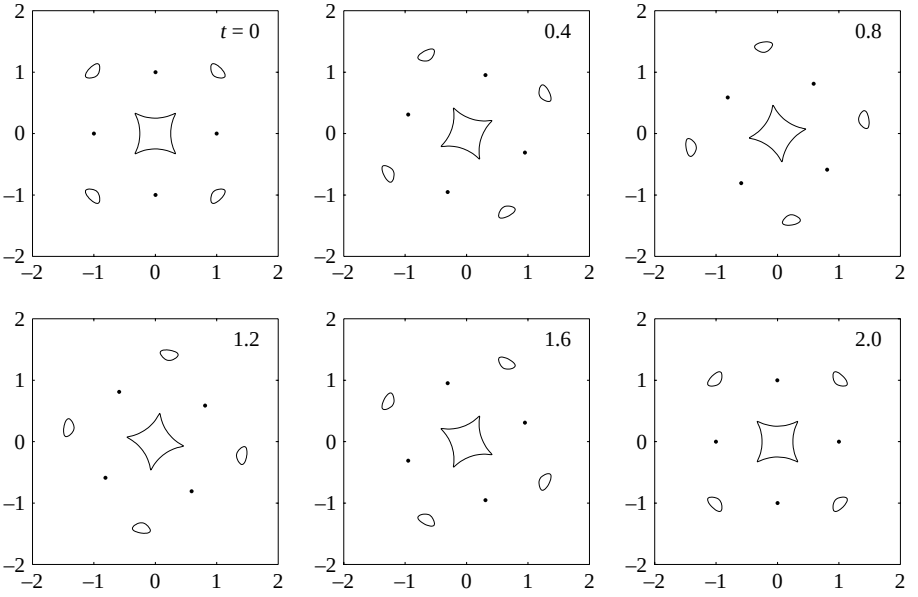

FIGURE 14. Snapshots of a contour dynamics simulation of a single revolution (at times $t = 0, (0.4), 2$) of the equilibrium of figure 5(b).

5. Contour dynamics simulations

While the final form of the conformal maps, (4.1), appears simple, the theory of automorphic functions leading to it is sophisticated and a check on the mathematical solutions seems appropriate. A useful check derives from the convenient feature of the equilibria that they are combinations of point vortices and vortex patches. Their full nonlinear evolution under the dynamics of the Euler equation can therefore be computed by straightforward adaptations of existing contour dynamics codes.

The contour surgery code due to Dritschel (1988) has been modified to include the effects of a finite distribution of point vortices interacting with the vortex patches. To check the mathematical solutions, this code is initialized using the vortex-patch boundaries, point-vortex positions and point-vortex circulations given by the analytical solutions above.

We take $\tilde{\omega} = 1$. Note that time has been rescaled with respect to 2π so that $t = 2$ corresponds to a single turnover time given that the angular velocity is $1/2$. Figures 14–16 show snapshots of the nonlinear evolution, during a single revolution, of initial conditions given by the equilibrium configurations shown in figures 5(b), 5(d) and 5(f), respectively. In figures 14 and 15 the vortex configurations are seen to be robust and simply rotate at a constant angular velocity without change of shape (a superposition of the initial and final configurations shows them to be indistinguishable). Longer-time integrations show that these configurations are very robust and do not change their form even after multiple turnovers. It is likely that these configurations are linearly stable. The calculations of figures 14 and 15 provide direct and independent verification of the correctness of the earlier mathematical analysis.

On the other hand, figure 16 suggests that the configuration in which the satellite vortex patches are so large that they have developed cusps at the points closest to the central vortex patch is unstable. Even within a single revolution, the satellite

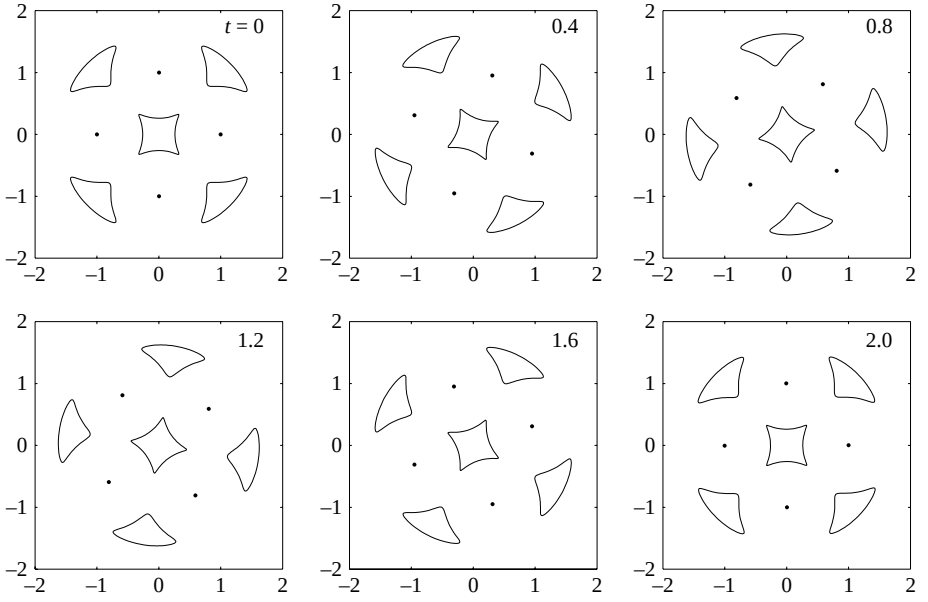

FIGURE 15. Snapshots of a contour dynamics simulation of a single revolution (at times $t = 0, (0.4), 2$) of the equilibrium of figure 5(d).

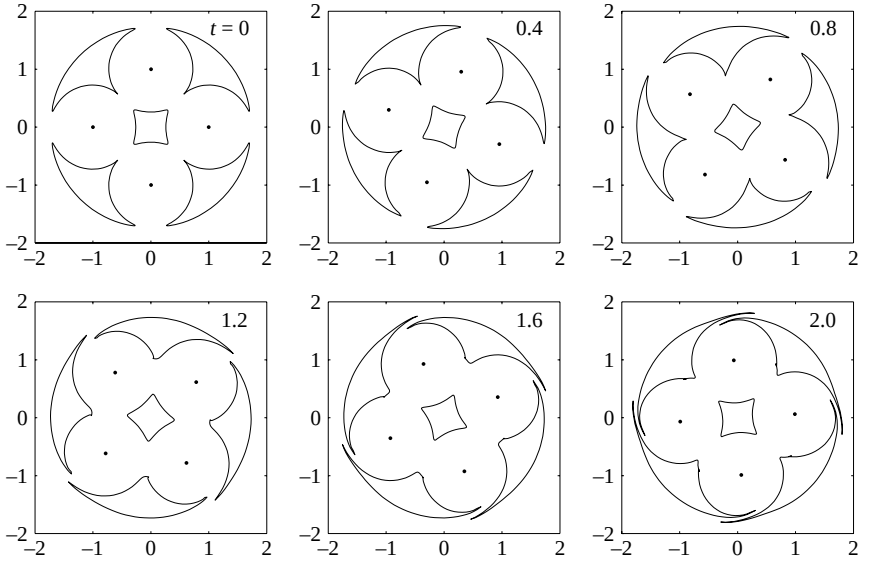

FIGURE 16. Snapshots of a contour dynamics simulation of a single revolution (at times $t = 0, (0.4), 2$) of the equilibrium of figure 5(f).

vortex patches exhibit an instability where their outermost boundaries become entrained in the circulatory flow with small filaments being drawn towards neighbouring patches.

To gain insight into the general robustness of the structures, some of the apparently stable structures are now perturbed to examine their subsequent evolution. Only perturbations to the point vortex positions are considered. Figure 17 shows the

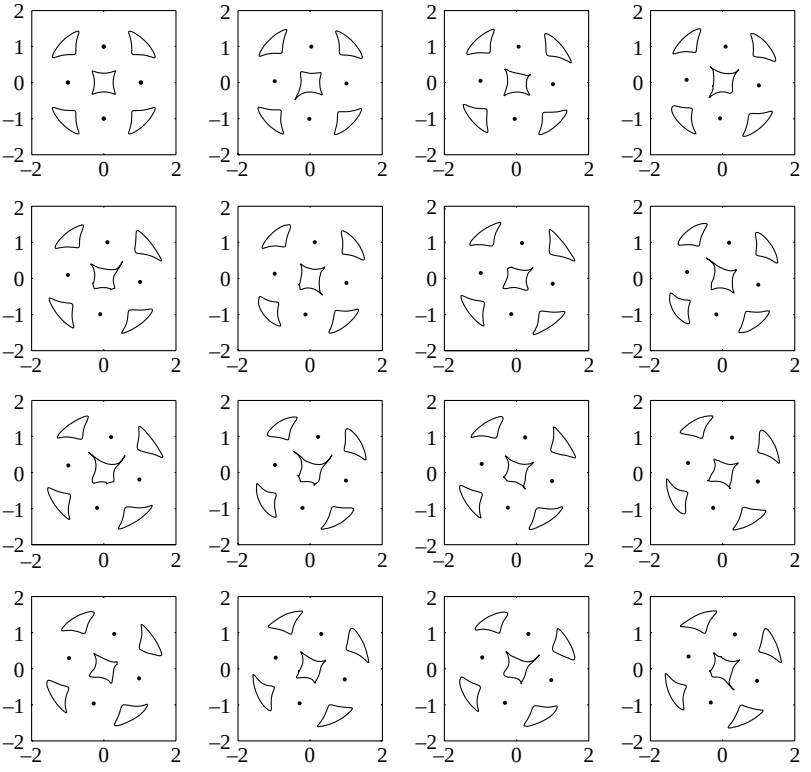

FIGURE 17. Snapshots of a contour dynamics simulation (at times $t = 0, (1), 15$) of the equilibrium in figure 5(d) perturbed by displacing the point vortex on the positive x-axis outwards by 0.025. This non-symmetric perturbation leads to a continual elongation and retraction of filaments of the central patch. No filamentation or stripping of vorticity is observed. Time increases to the right and down.

evolution of a non-symmetric perturbation in which just one of the point vortices is displaced outwards (we chose to displace the point vortex initially on the positive real axis to the right). Several different magnitudes of this displacement are examined. Figure 17 shows the case where the displacement is 0.025. Here, the central patch undergoes a repeating sequence in which protruding regions of the patch are drawn out into long thin filaments by the ambient straining flow. These filaments later retract back towards the centre of the patch. For a perturbation of 0.05, figure 18 shows that the perturbation is now sufficiently large that these long protruding filaments become so thin that they are excised from the central vortex patch by the contour surgery procedure (Dritschel 1988). These filamentation events recur continuously, but the overall vortical structure is robust and continues to rotate without significant change in the general distribution of the vorticity. In this way, vorticity is gradually stripped from the central vortex patch. The small excised filaments which are tossed around the configuration appear to have little dynamical effect and are sometimes observed to be completely removed by the surgery procedure. The filamentary debris is clearly visible in figure 18.

Figure 19 shows a symmetric perturbation in which all four satellite point vortices are displaced outwards by a distance of 0.05. The nature and magnitude of this perturbation also results in filamentation, this time involving both the central and

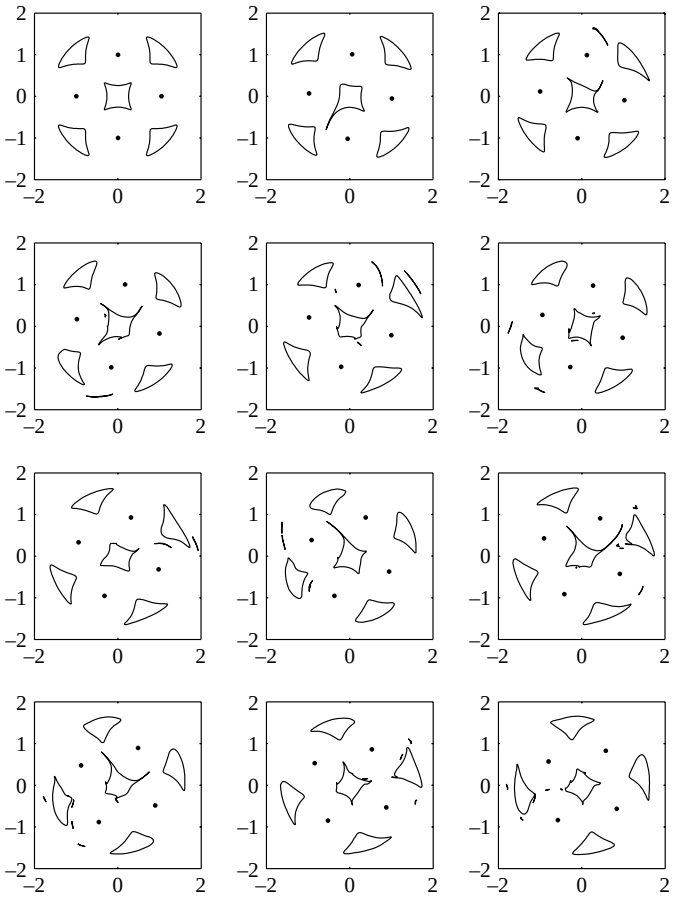

FIGURE 18. Snapshots of a contour dynamics simulation (at times $t = 0, (1), 11$) of the equilibrium in figure 5(*d*) perturbed by displacing the point vortex on the positive x-axis outwards by 0.05. This stronger non-symmetric perturbation leads to a continual filamentation mainly of the central patch. Notice that the total number of contours can also decrease as the surgery procedure removes the dynamically insignificant ones. Time increases to the right and down.

satellite vortex patches. Despite this gradual stripping of vorticity from the patches, the overall structure is robust.

5.1. *Point-vortex models*

The numerical simulations just performed suggest that, apart from finite-area effects such as the filamentation of the vortex patches, the overall vortical structures are robust and tend not to disintegrate immediately if the perturbations are sufficiently mild. To examine this quantitatively, we now devise 'point vortex' models of the new equilibria and study their stability. For the remainder of this paper, we shall refer to any instabilities of these point vortex models as 'displacement-mode instabilities'.

There are a number of ways to devise such models; here, we consider point-vortex models of the form shown schematically in figure 20. The model has the same qualitative distribution of circulations as the distributed-vorticity solutions and consists of a central point vortex of circulation Γ_{cp}, four satellite vortices at $\pm 1, \pm \mathrm{i}$ each of circulation Γ_s and four satellite vortices, each of circulation Γ_{sp} at positions $r\mathrm{e}^{\mathrm{i}(2k+1)\pi/4}$, $k = 0, 1, 2, 3$. Here, Γ_{cp}, Γ_s and Γ_{sp} are taken to be the values given by the class of analytical solutions found earlier. The distance r and the angular velocity Ω_{pv}

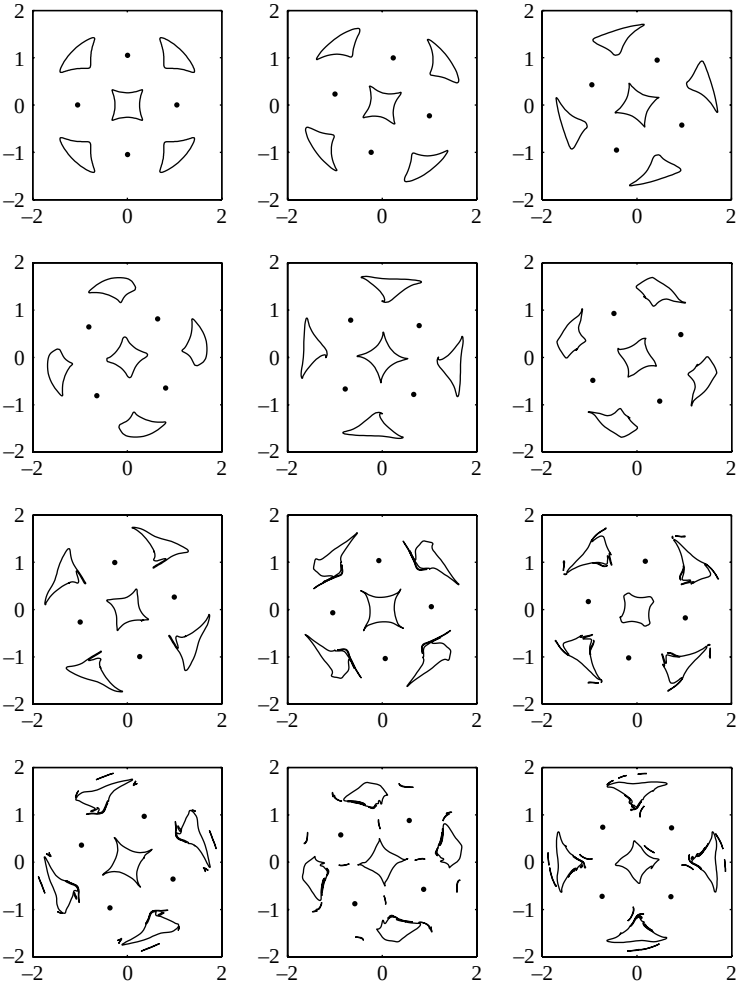

FIGURE 19. Snapshots of a contour dynamics simulation (at times $t = 0, (1), 11$) of the equilibrium in figure 5(*d*) perturbed by moving all point vortices outwards by 0.05. This symmetric perturbation leads to filamentation of both satellite and central patches, but the overall structure remains robust. Time increases to the right and down.

of the rotating point vortex configuration, are found by solving the two conditions that ensure that the configuration is rotating steadily, without change of form, at angular velocity Ω_{pv}. These two conditions can be imposed by moving to a frame of reference rotating about the origin with angular velocity Ω_{pv} and then insisting that the point vortices at distances 1 and r from the origin are stationary in such a frame. Symmetry dictates that there are only two such conditions. Of course, the combined vortex-patch/point vortex solutions found earlier all rotate with angular velocity 1/2 while the distance r_C, say, of the centroid of the satellite patches from the origin can easily be computed from the solution class using the formula

$$r_C = \left| \frac{\oint_{\partial H_1} z(\zeta)\overline{z}(\zeta^{-1}) z_\zeta \, \mathrm{d}\zeta}{\oint_{\partial H_1} \overline{z}(\zeta^{-1}) z_\zeta \, \mathrm{d}\zeta} \right|. \tag{5.1}$$

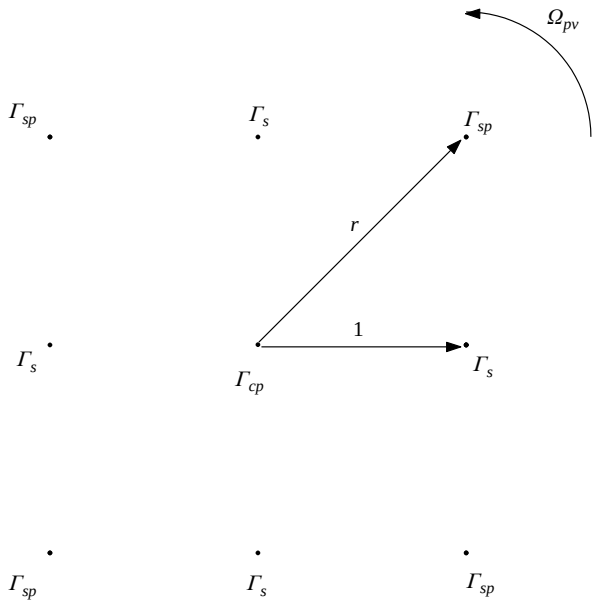

FIGURE 20. Schematic of a point-vortex model.

q	r_C	r	Ω_{pv}
0.025	1.430	1.427	0.500
0.05	1.432	1.419	0.502
0.075	1.442	1.410	0.510
0.1	1.460	1.406	0.526

TABLE 1. The values of r_C, r and Ω_{pv} for $\alpha = 2.8$ and various choices of q.

To justify the model, table 1 shows some typical values of r_C, r and Ω_{pv} for $\alpha = 2.8$ and for various values of q. It is clear that the values of r are close to r_C, while Ω_{pv} remains close to $1/2$. This forms the basis of our assertion that the linear stability of the point-vortex models (which is straightforward to calculate) provides a good estimate of whether the new solution class is susceptible to disintegration due to displacement modes. In the language of Aref & Vainchtein (1998), the point-vortex model is an example of a 'staggered 4–4' array with a central point vortex. A straightforward linear stability analysis of the point-vortex models associated with the configurations in figures 5 and 7 reveals that they are all linearly stable. This calculation involves finding the eigenvalues of an 18×18 matrix associated with horizontal and vertical displacements of the 9 point vortices making up the point-vortex configuration. This result is consistent with the general robustness of the new vortex structures observed in the contour dynamics simulations and suggests that the configurations are (linearly) stable to displacement modes, even though it says nothing about whether finite-area and/or nonlinear effects will eventually destabilize the configurations. The instability observed in figure 16 is probably attributable to a finite area effect rather than to a displacement-mode instability.

All this evidence suggests that the vortex arrays are structurally robust and that many are linearly stable. It seems reasonable to conjecture that, if perturbations are

sufficiently mild, one of the ways in which destabilization may eventually occur is in a nonlinear fashion where, over long periods, filamentation and stripping of vorticity from the patches may ultimately change the distribution of circulations sufficiently that the configuration becomes unstable to displacement-mode instabilities leading to destruction of the array.

6. Pure-patch quasi-equilibria

Having just considered pure point-vortex models (with no patches) of the new solutions, we now consider the opposite scenario of pure-patch equilibria containing no point vortices. The idea of desingularizing a point vortex and replacing it with a uniform vortex patch is well-known: Dritschel (1985), for example, has computed the finite-area analogues of the Thomson polygonal point-vortex arrays. It is conceivable that the configurations found in this paper can be 'continued' to a configuration consisting purely of vortex patches by desingularizing the satellite point vortices. This would have to be done numerically, but the present solutions should provide valuable non-trivial initial conditions for a numerical procedure (e.g. based on Newton's method) for constructing such equilibria using continuation.

While we do not attempt such a numerical construction here, we present numerical evidence of the viability of constructing pure-patch equilibria in this way. Note that in certain of the exact solutions just obtained, the streamlines surrounding the point vortices can be very close to circular, even at relatively large distances from the point-vortex positions. This is clear, for example, from the last few diagrams in figures 5 and 7 where the boundaries of the vortex patches assume the shape of near-circular arcs, thus suggesting that the streamlines close to them are also close to circular. This suggests the possibility of obtaining a near-equilibrium configuration, or 'quasi-equilibrium', by replacing the point vortices in the exact solutions by Rankine vortices of the same total circulation.

To test this possibility, figure 21 shows a contour dynamics simulation where the initial condition is given by that of figure 5(*d*) except that the satellite point vortices have been replaced by Rankine vortices of radius 0.2 and with the same total circulation as the original point vortices. The calculation is performed for sixteen turnover times of the unperturbed equilibrium. Since this is not an exact equilibrium, the smearing out of the point vortices to Rankine vortices can be interpreted as a perturbation to the exact solution which, as in previous calculations, leads to the formation of thin filaments and even vortex stripping. It is also clear that the angular velocity of the configuration has changed. Nevertheless, it is remarkable that, even after such long times, the overall distribution of the vorticity is very close to its original state. Indeed, the Rankine vortices remain close to circular throughout the entire calculation. The existence of this robust pure-patch vortical structure provides evidence of the possibility of numerically continuing the exact solution class presented here to a class of pure-patch equilibria of the Euler equation by desingularizing the point vortices.

7. Discussion

By using a single special function $\omega(\zeta, \gamma)$, conformal mappings of the functional form (4.1) have been constructed which map a region H to the irrotational region D exterior to $N+1$ co-existing vortex patches in equilibrium under the dynamics of the Euler equation. Being a combination of point vortices and vortex patches, the solutions provide a convenient forum for studying the interaction of finite-area effects

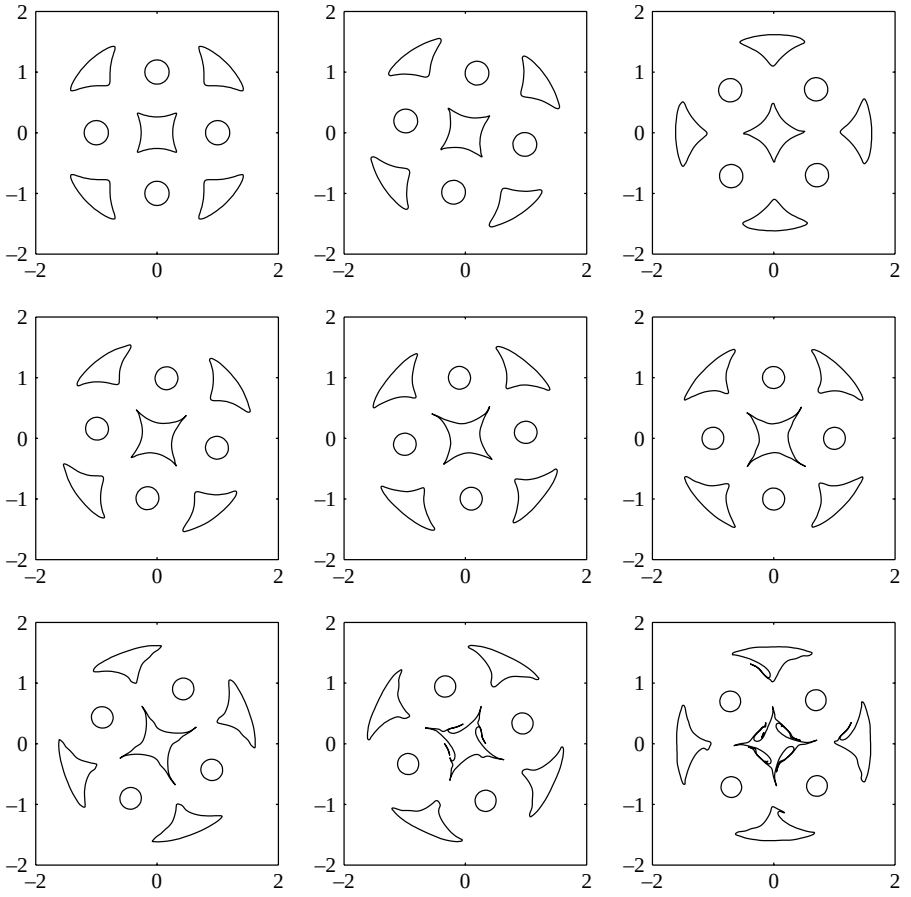

FIGURE 21. A pure-patch quasi-equilibrium in which the point vortices of the exact equilibrium of figure 5(*d*) are replaced by Rankine vortices of radius 0.2. The uniform vorticity of the central patch and the umbrella-shaped satellite patches is 1, the uniform vorticity of the Rankine vortices is $\Gamma_s/(0.04\pi) = 13.95$. Times shown at $t = 0, (4), 32$. The overall structure appears to be relatively robust.

with displacement-mode effects. Many of the configurations are structurally robust and a possible nonlinear destabilization mechanism has been proposed whereby an original array which is stable to displacement-mode instabilities (as reflected in the linear stability of the proposed 'point-vortex models') may eventually be destroyed as a result of long-time stripping of vorticity from the patches to a situation where the distribution of circulations is such that the configuration becomes unstable to displacement-mode instabilities. A full investigation of the stability of the new equilibria is left for the future, but it should be pointed out that a detailed analysis of the linear stability of the solutions corresponding to $q = 0$ (when the satellite vortex patches disappear) has already been performed in Crowdy (2002) and many of the configurations prove to be linearly stable structures.

The solutions can be interpreted as being formed by 'growing' small co-rotating satellite vortex-patch regions at the co-rotation points of the known equilibria derived in Crowdy (2002) (which involve just a single central patch). This develops an idea first proposed and implemented by Aref & Vainchtein (1998) who grew new point

vortices at the co-rotation points of various point vortex equilibria. There appears to be no mathematical analysis that guarantees the success of growing a patch at a given co-rotation point of an existing equilibrium, but it is sometimes possible as has been seen by direct construction. Aref & Vainchtein (1998) also identify some asymmetric point-vortex equilibria. While we have not sought them here, it should be mentioned that our general analytical approach can, in principle, be extended to find asymmetric equilibria involving combinations of point vortices and vortex patches. However, the functional form of the map (4.1) would then become more complicated.

There have been many recent advances in the construction of vortical equilibria of the Euler equation. The device of 'growing' vortex patches used here suggests possibilities for the future construction of new vortical equilibria based on combined point-vortex and vortex-patch models. We note here that the present authors Crowdy & Marshall (2004*b*) have explored the idea of 'growing' new vortex patches in a simpler analytical environment (which does not require the full machinery of automorphic functions used here) and shown that the simple co-rotating point-vortex pair is connected to the simple Rankine vortex solution by a continuous branch of exact solutions. By procedures such as (i) the desingularization of point vortices to uniform vortex patches (or vice versa); (ii) the growing of new point vortices at co-rotation points of existing equilibria as done by Aref & Vainchtein (1998); (iii) the growing of new vortex patches at co-rotation points of existing equilibria as done here; and (iv) the smooth continuation of touching vortex patches to a merged equilibrium as done by Cerretelli & Williamson (2003), it appears that even basic equilibria with simple vorticity distributions can be continously continued to more complicated ones with more elaborate vortical topology.

Another very general method of constructing analytical solutions of the Euler equation was presented by Abrashkin & Yakubovich (1984). Their method relies on a Lagrangian formulation of the equations and yields a class of unsteady solutions depending biharmonically on time and on two arbitrary analytic functions. Their solution class contains the exact solutions of Kirchhoff (Saffman 1992) and Gerstner (Lamb 1993) as special cases. The connection between their constructive method and that developed here is not yet clear, but it is likely that our solutions will be retrievable by appropriate choices of the arbitrary functions appearing in the formulation of Abrashkin & Yakubovich (1984). To elucidate such a connection is likely to throw much light on the theory of vortical solutions of the Euler equations and is an intriguing open question.

For the generalized solutions to be describable in terms of the mathematical formulae given here, the new vortex patches have been taken to be in pure solid-body rotation with the same angular velocity as the original rotating configuration. This is so that the resulting streamfunction is a modified Schwarz potential – a class of streamfunctions first shown by Crowdy (1999) to have attractive mathematical properties in that the vortex-patch boundaries and point-vortex positions, as well as the associated velocity field generated by the vortical configuration, can be written down in terms of mathematical formulae with no need for numerical determination of the patch boundaries or use of a Biot-Savart integral to determine the velocity field. It is expected that more general vortex patches (i.e. those not necessarily in solid-body rotation, but with non-trivial irrotational components) can also be grown at co-rotation points using more general methods, but probably at the cost of losing a description in terms of mathematical formulae.

The new solutions are expected to provide non-trivial equilibria from which other equilibria might be derived using numerical continuation procedures. The idea of

desingularizing the point vortices has already been discussed in § 6. Another possibility is to find numerical solutions corresponding to gradually decreasing Γ_s to see if pure-patch solutions consisting of a central patch surrounded by N satellite patches can be constructed. For the intermediate solutions, the vortex patches are likely not to be in pure solid-body rotation. Also, neighbouring non-symmetric solutions (with, for example, different-sized satellite vortex patches) may also be available by continuation from the solutions herein.

Even though the literature concerning the numerical study of multi-vortex-patch interactions is extensive, to the best of our knowledge, the new solutions are believed to be the first examples of analytical solutions involving an essentially arbitrary finite number (i.e. $N+1$ where $N \geqslant 3$) of interacting vortex patches. Finally, it is natural is ask about another interesting limit of the solution class where $N \to \infty$ so that there are an arbitrarily large number of alternating point vortices and vortex patches in an annular ring around a central patch. The investigation of this asymptotic limit does not appear to be straightforward and is left for the future.

This work is supported in part by a grant from EPSRC. J. M. acknowledges the support of an EPSRC studentship.

Appendix A. The special function $\omega(\zeta, \gamma)$

The conformal maps (4.1) depend on just one special function $\omega(\zeta, \gamma)$. In this section, we show how to construct $\omega(\zeta, \gamma)$ explicitly in the case $N = 4$. The construction for other N is analogous to the treatment below. The function $\omega(\zeta, \gamma)$ is known as the *Schottky–Klein prime function*. For more details on the background theory, see Crowdy & Marshall (2004*a*) or Baker (1995). This Appendix is supposed to be self-contained, including enough details for the reconstruction of the mapping functions (4.1) with only brief details of their derivation.

In the $N = 4$ example considered in § 4, we must have

$$z(\zeta) = z(\theta_j(\zeta)) \quad \text{for } j = 1, \ldots, 4, \tag{A 1}$$

where the four Möbius maps θ_j, $j = 1, \ldots, 4$ are explicitly given by

$$\left.\begin{aligned}
\theta_1(\zeta) &= \delta \mathrm{e}^{\mathrm{i}\pi/4} + \frac{q^2\zeta}{\left(1 - \delta e^{-i\pi/4}\zeta\right)}, \\
\theta_2(\zeta) &= \delta \mathrm{e}^{3\mathrm{i}\pi/4} + \frac{q^2\zeta}{\left(1 - \delta e^{-3i\pi/4}\zeta\right)}, \\
\theta_3(\zeta) &= \delta \mathrm{e}^{5\mathrm{i}\pi/4} + \frac{q^2\zeta}{\left(1 - \delta e^{-5i\pi/4}\zeta\right)}, \\
\theta_4(\zeta) &= \delta \mathrm{e}^{7\pi\mathrm{i}/4} + \frac{q^2\zeta}{\left(1 - \delta e^{-7i\pi/4}\zeta\right)}.
\end{aligned}\right\} \tag{A 2}$$

They depend on just two real parameters, q and δ. See figure 3 for a schematic.

Using these four basic maps, we can construct an infinite number of Möbius maps by composition (a composition of two Möbius maps is easily shown to yield another Möbius map). This infinite set of Möbius maps will be required in the construction of $\omega(\zeta, \gamma)$. It is convenient to categorize all possible compositions of these four maps according to their level. The identity map is considered to be the level-zero map. The four maps (A 2) together with their inverses (which are also Möbius maps – a fact

that is easily verified) constitute the eight level-one maps. All possible combinations of any two of these eight level-one maps, e.g.

$$\theta_1(\theta_1(\zeta)),\quad \theta_1(\theta_2(\zeta)),\quad \theta_1(\theta_3(\zeta)),\quad \theta_1(\theta_4(\zeta)),\quad \theta_2(\theta_1(\zeta)),\quad \theta_2(\theta_2(\zeta)),\ldots \tag{A 3}$$

will be called the level-two maps, all possible combinations of any three of the eight level-one maps, (A 2), will be called the level-three maps, and so on.

Now, $\omega(\zeta,\gamma)$ is defined as

$$\omega(\zeta,\gamma)=(\zeta-\gamma)\prod_{\{\theta_i\}}\frac{(\theta_i(\zeta)-\gamma)(\theta_i(\gamma)-\zeta)}{(\theta_i(\zeta)-\zeta)(\theta_i(\gamma)-\gamma)}, \tag{A 4}$$

where the notation $\{\theta_i\}$ denotes a product over all possible Möbius maps whose construction has just been described, excluding the identity and all inverse maps. This means that if, for example, $\theta_1(\theta_2(\zeta))$ is included, then the map $\theta_2^{-1}(\theta_1^{-1}(\zeta))$ must be excluded. Note from the definition (A 4) that $\omega(\zeta,\gamma)$ has a simple zero at $\zeta=\gamma$.

If γ should equal infinity, then we instead define

$$\omega(\zeta,\infty)=\prod_{\{\theta_i\}}\frac{(\theta_i(\infty)-\zeta)}{(\theta_i(\zeta)-\zeta)}. \tag{A 5}$$

The central result used in this paper in the construction of the map (4.1) is now stated without proof (for more details, see Baker 1995). According to the general theory, $\omega(\zeta,\gamma)$ can be used to construct automorphic functions. Indeed, if $\{\alpha_k\in\mathbb{C}|k=1,\ldots,M\}$ and $\{\beta_k\in\mathbb{C}|k=1,\ldots,M\}$ denote two sets of complex parameters and $R\in\mathbb{C}$, then

$$f(\zeta)=R\frac{\prod_{k=1}^{M}\omega(\zeta,\beta_k)}{\prod_{k=1}^{M}\omega(\zeta,\alpha_k)} \tag{A 6}$$

is an automorphic function provided that the parameters satisfy algebraic conditions which are referred to in this paper as *automorphicity conditions*. Since $f(\zeta)$ vanishes when $\zeta=\beta_k, k=1,\ldots,M$ and goes to infinity when $\zeta=\alpha_k, k=1,\ldots,M$, the set $\{\beta_k\in\mathbb{C}|k=1,\ldots,M\}$ are *zeros* of $f(\zeta)$ and $\{\alpha_k\in\mathbb{C}|k=1,\ldots M\}$ are *poles* of $f(\zeta)$.

The map (4.1) has been constructed using this general theory. Indeed, (4.1) takes precisely the form (A 6). In this case $N=4$, we choose $M=5$. This is because $\zeta=0$ is a pole of the mapping (mapping to $z=\infty$) while we must have four poles corresponding to the four point vortices (for all other N, $M=N+1$). The five parameters $\{\alpha_k\in\mathbb{C}|k=1,\ldots,5\}$ are then given by

$$\{0,\alpha,\mathrm{i}\alpha,-\alpha,-\mathrm{i}\alpha\}, \tag{A 7}$$

while the five parameters $\{\beta_k\in\mathbb{C}|k=1,\ldots,5\}$ are given by

$$\{\infty,\beta,\mathrm{i}\beta,-\beta,-\mathrm{i}\beta\}. \tag{A 8}$$

Note that this choice of poles and zeros possesses the same four-fold rotational symmetries in the ζ-plane as the required physical configuration in the z-plane.

Owing to the high degree of symmetry in the maps (4.1), there is just one automorphicity condition to be satisfied (for a general domain H with four holes but no symmetries there would be four such conditions. Here, the four such conditions reduce to the same single condition). This is given by

$$\prod_{j=1}^{N}\prod_{\theta_i\in\Theta_1}\frac{(\alpha_j-\theta_i(B))}{(\alpha_j-\theta_i(A))}\Big/\frac{(\beta_j-\theta_i(B))}{(\beta_j-\theta_i(A))}=1, \tag{A 9}$$

where A and B are the fixed points of θ_1, i.e. the two solutions of the quadratic equation $\theta_1(\zeta) = \zeta$ and the second product is taken over the set Θ_1 defined to be the identity map plus all possible Möbius mappings generated by the maps $\theta_1, \ldots, \theta_4$ and their inverses, excluding any maps having a power of θ_1 on the right-hand end.

Putting all this together, the mapping is

$$z(\zeta) = R\frac{\omega(\zeta,\infty)\omega(\zeta,\beta)\omega(\zeta,\mathrm{i}\beta)\omega(\zeta,-\beta)\omega(\zeta,-\mathrm{i}\beta)}{\omega(\zeta,0)\omega(\zeta,\alpha)\omega(\zeta,\mathrm{i}\alpha)\omega(\zeta,-\alpha)\omega(\zeta,-\mathrm{i}\alpha)}. \tag{A 10}$$

A more concise way to write this function is to introduce the notation

$$\omega_N(\zeta,\gamma) = \prod_{j=1}^{N}\omega\left(\zeta,\gamma\mathrm{e}^{2\pi\mathrm{i}(j-1)/N}\right), \tag{A 11}$$

so that (A 10) becomes

$$z(\zeta) = R\frac{\omega(\zeta,\infty)\omega_4(\zeta,\beta)}{\omega(\zeta,0)\omega_4(\zeta,\alpha)}, \tag{A 12}$$

which is precisely the form (4.1) with $N = 4$.

On a practical note, to write a function routine to calculate $\omega(\zeta,\gamma)$ numerically, it is necessary to truncate the infinite product in (A 4). This is done in a very natural way by including all Möbius maps up to some chosen level and truncating the contribution to the product from all higher-level maps. The truncation which includes all level-zero, level-one and level-two maps is found to be very accurate for the class of maps (4.1) and all figures produced in this paper were prepared using this truncation. A good test of the accuracy of any chosen truncation is how well the resulting maps satisfy (A 1) for arbitrary choices of ζ.

Appendix B. The stationarity condition

The velocity field associated with the exact solutions is given explicitly as a function of $\zeta, \bar{\zeta}$ by the formula

$$u - \mathrm{i}v = \frac{\mathrm{i}\tilde{\omega}R}{2}\left(\frac{\omega(\bar{\zeta},\infty)\omega_N(\bar{\zeta},\beta)}{\omega(\bar{\zeta},0)\omega_N(\bar{\zeta},\alpha)} - \frac{\omega(\zeta^{-1},\infty)\omega_N(\zeta^{-1},\beta)}{\omega(\zeta^{-1},0)\omega_N(\zeta^{-1},\alpha)}\right). \tag{B 1}$$

This equation can be used to find a formula for Γ_s and the stationarity condition. Equation (B 1) takes the general form

$$u - \mathrm{i}v = \frac{\mathrm{i}\tilde{\omega}R}{2}\left(\frac{A(\zeta)}{\zeta - \alpha^{-1}} + B(\bar{\zeta})\right), \tag{B 2}$$

where explicit formulae for $A(\zeta)$ and $B(\bar{\zeta})$ can be derived from (B 1).

Let z_1 denote the position of the point vortex on the positive real axis. Then, $z_1 = z(\alpha^{-1})$ and

$$z - z_1 = z_\zeta(\alpha^{-1})(\zeta - \alpha^{-1}) + \frac{z_{\zeta\zeta}(\alpha^{-1})}{2}(\zeta - \alpha^{-1})^2 + \ldots, \tag{B 3}$$

so that

$$\frac{1}{\zeta - \alpha^{-1}} = \frac{z_\zeta(\alpha^{-1})}{z - z_1} + \frac{z_{\zeta\zeta}(\alpha^{-1})}{2z_\zeta(\alpha^{-1})} + O(z - z_1). \tag{B 4}$$

Using this, it follows that the circulation Γ_s of the point vortex is

$$\Gamma_s = -\pi\tilde{\omega}RA(\alpha^{-1})z_\zeta(\alpha^{-1}), \tag{B 5}$$

while the stationarity condition takes the form

$$A_\zeta(\alpha^{-1}) + A(\alpha^{-1})\frac{z_{\zeta\zeta}(\alpha^{-1})}{2z_\zeta(\alpha^{-1})} + B(\alpha^{-1}) = 0. \tag{B 6}$$

REFERENCES

Ablowitz, M. A. & Fokas, A. S. 1997 *Complex Variables*. Cambridge University Press.

Abrashkin, A. A. & Yakubovich, E. I. 1984 Planar rotational flows of an ideal fluid. *Sov. Phys. Dokl.* **29**, 370.

Aref, H., Newton, P. K., Stremler, M. A., Tokieda, T. & Vainchtein, D. L. 2002 Vortex crystals. *Adv. Appl. Mech.* **39**, 1–79.

Aref, H. & Vainchtein, D. L. 1998 Point vortices exhibit asymmetric equilibria. *Nature* **392**, 769–770.

Baker, H. 1995 *Abelian Functions*. Cambridge University Press.

Bauer, L. L. & Morikawa, G. K. 1976 Stability of rectilinear geostrophic vortices in stationary equilibrium. *Phys. Fluids* **19**, 929–942.

Carnevale, G. F. & Kloosterziel, R. C. 1994 Emergence and evolution of triangular vortices. *J. Fluid Mech.* **259**, 305.

Cerretelli, C. & Williamson, C. H. K. 2003 A new family of uniform vortices relating to vortex configurations before merging. *J. Fluid Mech.* **493**, 219.

Crowdy, D. G. 1999 A class of exact multipolar vortices. *Phys. Fluids* **11**(9), 2556–2564.

Crowdy, D. G. 2002 Exact solutions for rotating vortex arrays with finite-area cores. *J. Fluid Mech.* **469**, 209–235.

Crowdy, D. G. & Marshall, J. S. 2004*a* Constructing multiply-connected quadrature domains. *SIAM J. Appl. Math.* **64**, 1334–1359.

Crowdy, D. G. & Marshall, J. S. 2004*b* Growing vortex patches. *Phys. Fluids* **16**, 3122–3129.

Davis, P. J. 1974 *The Schwarz Function and its Applications*. Carus Mathematical Monographs.

Dritschel, D. G. 1985 The stability and energetics of corotating uniform vortices. *J. Fluid Mech.* **157**, 95–134.

Dritschel, D. G. 1988 Contour surgery: a topological reconnection scheme for extended integrations using contour dynamics. *J. Comput. Phys.* **77**, 240–266.

Durkin, D. & Fajans, J. 2000 Experiments of two-dimensional vortex patterns. *Phys. Fluids* **12**, 289.

Havelock, T. H. 1931 The stability of motion of rectilinear vortices in ring formation. *Phil. Mag.* (Ser. 7), **1**, 617–633.

Lamb, H. 1993 *Hydrodynamics*, 6th edn. Cambridge University Press.

Melander, M. V., Zabusky, N. J. & Styczek, A. S. 1986 A moment model for vortex interactions of two-dimensional Euler equations. Part 1. Computational validation of a Hamiltonian elliptical representation. *J. Fluid Mech.* **167**, 95–115.

Morel, Y. G. & Carton, X. J. 1994 Multipolar vortices in two-dimensional incompressible flows. *J. Fluid Mech.* **267**, 23.

Morikawa, G. K. & Swenson, E. V. 1971 Interacting motion of rectilinear geostrophic vortices. *Phys. Fluids* **14**, 1058–1073.

Morton, W. B. 1933 On some permanent arrangements of parallel vortices and their points of relative rest. *Proc. R. Irish Acad.* A **41**, 94–101.

Newton, P. K. 2001 *The N-Vortex Problem*. Springer.

Saffman, P. G. 1992 *Vortex Dynamics*. Cambridge University Press.

Saffman, P. G. & Pullin, D. I. 1996 Calculation of velocity structure functions for vortex models of isotropic turbulence. *Phys. Fluids* **8**, 3072.

Schecter, D. A., Dubin, D. H. E., Fine, K. S. & Cass, A. C. 1999 Vortex crystals from 2D Euler flow: experiment and simulation. *Phys Fluids* **11**, 905.

Shapiro, H. S. 1992 *The Schwarz Function and its Generalization to Higher Dimension*. Wiley.

Thomson, J. J. 1883 On the motion of vortex rings (Adams Prize Essay). Macmillan.